Asian Journal of Research in Biological and Pharmaceutical Sciences

Journal home page: www.ajrbps.com

CLEMATIS GOURIANA ROXB. EX DC COMPOUNDS COULD BE POTENT INHIBITS FOR SNAKE VENOM METALLOPROTEINASE (SVMP) A MOLECULAR DOCKING AND SIMULATION STUDIES

Karthikeyan Muthusamy*[1], Sathishkumar Chinnasamy[1], Pappathi Palanisamy[1], Gopinath Krishnasamy[1]

[1]*Department of Bioinformatics, Alagappa University, Karaikudi, Tamil Nadu, India.

ABSTRACT

Snake venom metalloproteinase (SVMP) is abundant in snake venom toxins and plays a vital role in snake venom envenomation, including hemorrhagic, fibrigenolytic, and myotoxic effects in the victims. SVMP is regulated by metal ions (Zn^{2+} and Ca^{2+}) and plays a critical role in many catalytic mechanisms and structural properties. In this study, SVMP was modeled with Zn^{2+} and Ca^{2+} ions. Molecular docking, prime/MM-GBSA (DG_Bind calculations), quantum polarized ligand docking (QPLD), quantum mechanical and molecular mechanical interaction energy analysis, and molecular dynamics simulation were performed for the compounds SID 249494133, SID 249494134, and SID 249494135 with SVMP in the presence and absence of metal ions (Zn^{2+} and Ca^{2+}). The results show that these compounds interact greatly with HIS138, GLU139, HIS142, and HIS148, owing to the presence of ions in the protein. The ions induce conformational changes and atomistic movements in the SVMP protein. Zn^{2+} and Ca^{2+} ions performed cuticle functions in the ligand binding of the SVMP protein.

KEYWORDS

Anti-venom, Molecular docking, DFT and MD simulation.

Author for Correspondence:

Karthikeyan Muthusamy,
Department of Bioinformatics,
Alagappa University,
Karaikudi, Tamil Nadu, India

Email: mkbioinformatics@gmail.com

INTRODUCTON

Snake venom is a rich source of proteins and peptides that induce a large variety of pharmacological and toxic effects such as edema, vascular clotting, hemorrhage, and necrosis (Fox and Serrano, 2009[1], Laraba-Djebari Fatima and Chérifi Fatah, 2014[2], Ramos Selistre-de-Araujo, 2006)[3]. Systemic disorders such as coagulopathies and hemorrhage are the major symptoms associated snakebite in humans. Snake venom

metalloproteinase (SVMP) is a major component of snake venom (Sajevic *et al.,* 2011)[4]. Particularly, the zinc-dependent SVMP with a large structural similarity to the zinc-binding domain plays an important role in hemorrhage and local tissue damage (Gasanov *et al.,* 2014)[5]. It is responsible for the syndrome in snake envenomation (Huang *et al.,* 2002[6], Mendes *et al.,* 2013)[7], which one of the most serious consequences of a snakebite (Gutierrez *et al.,* 2005)[8]. SVMP is regulated by different mechanisms such as activating apoptotic or pro-inflammatory activates, disruption of hemostasis mediated pro- or anticoagulant effects (prothrombin, fibrinogenase, and fibrolase), and platelet aggregation inhibitors (Markland, 1998[9], Kini and Evans 1992[10], Escalante *et al.,* 2011)[11]. The zinc-dependent SVMP causes hemorrhagic effects, myonecrosis, skin damage, edema, and other associated inflammations as well as relevant homeostatic and hematological alterations (Bjarnason Fox, 1994[12], Rucavado *et al.,* 1998[13], Gutierrez *et al.,* 2005)[8]. Zinc-dependent SVMP directly affects the integrity of microvessels, particularly capillaries (Gutierrez *et al.,* 2005)[8], and induces the hemorrhagic effect (Gutiérrez *et al.,* 2016)[14]. The hemostatic and microvessel disturbances act synergistically to provoke profuse bleeding in snake envenomation (Kamiguti *et al.,* 1992[15], Escalante *et al.,* 2003)[16]. The hemorrhagic toxins autonomously induce bleeding in the absence of hemostatic alterations (Gutierrez *et al.,* 2005)[8]. Thus, some of these SVMP contain applications for treating human conditions involving abnormal blood clotting (Han *et al.,* 2010[17], Gasanov*et al.,* 2014)[5]. SVMP involved in the additional mechanism of hemorrhage is caused by the base membrane and disturbs the interactions between the endothelial cells through the degradation of endothelial cell membrane proteins (e.g., integrin, cadherin) (Takeda *et al.,* 1824)[18] and basement membrane components (e.g., fibronectin, laminin, nidogen, type IV collagen) (Baramova *et al.,* 1989[19], Kim Baeten *et al.,* 2011)[20].

SVMP is an element of metazincins, a family of zinc-dependent metallopeptides that present two main features: (i) the extended motif of the active site HEXXHXXGXXHD with three histidines as zinc ligands and (ii) a Met-turn with a conservative

methionine located in a 1, 4-ß-loop. This methionine was located downstream of the consensus sequence provides a hydrophobic basement for the three zinc-binding imidazoles. Besides the catalytically important zinc ion, these enzymes also have calcium ions on the surface of the molecule, which is important for providing structural stability to the catalytic domain (Gutierrez, 2005)[8]. In this study, the zinc-dependent SVMP (*Echiscoloratus* (*Carpet viper*)) modeled protein (Chinnasamy *et al.,* 2014)[21] was used for analysis. Molecular docking study was performed for the molecules SID 249494133, SID 249494134, and SID 249494135 with SVMP in the presence and absence of metals (Zn^{2+} and Ca^{2+}). Prime/MM-GBSA (ΔG_{Bind}) calculations and quantum polarized ligand docking (QPLD) analyses were performed for SVMP in the presence and absence of metals (Zn^{2+} and Ca^{2+}). Furthermore, the docking studies were supported by quantum mechanical and molecular mechanical (QM–MM) interaction energy analysis. In addition, the stability of the protein-ligand complexes was performed by MD simulation using Desmond.

The Compounds denoted following PubChem Ids were SID 249494133, SID 249494134, and SID 249494135 was isolated from *Clematis gouriana* Roxb. ex DC (Supplementary Figure No.1-3). The structures were solved on the basis of their ^{1}H NMR, ^{13}C NMR, LCMS, HRESIMS and FT-IR data. These structures were submitted to PubChem compound database (Muthusamy *et al.,* 2016)[22].

MATERIAL AND METHODS
Protein preparation
The SVMP was prepared by protein preparation wizard (Schrödinger, LLC, New York, NY, 2014) in the presence of Zn^{2+} and Ca^{2+} ions (combination 1), in the absence of Zn^{2+} and Ca^{2+} ions (combination 2), in the absence of Ca^{2+} but in the presence of Zn^{2+} ion (combination 3), and in the absence of Zn^{2+} and in the presence of Ca^{2+} ion (combination 4) with the protein. Each model was energy minimized using OPLS-2005 force field (Optimized Potentials for Liquid Simulations). Progressively weaker restraints were applied to the non-hydrogen atoms and the refinement procedure was performed based on the recommendation of

Schrödinger LLC (Schrödinger, LLC, New York, NY, 2015) as Glide used the full OPLS-2005 force field at an intermediate docking stage and claimed to be more sensitive to geometric details than other docking tools. The thiol hydrogen atoms and the most likely positions of hydroxyl, protonation states and tautomers of HIS residues, and Chi 'flip' assignments for ASN, GLN, and HIS residues were selected using the protein assignment script shipped by Schrödinger. The minimizations were performed until the average root mean square deviation of the non-hydrogen atoms reached 0.3 Å.

Ligand preparation
The molecules of SID 249494133, SID 249494134, and SID 249494135 were drawn in Maestro (Schrödinger, LLC, New York, NY, USA) and assigned the structure using the LigPrip package from Schrödinger, LLC, New York, NY, USA. This structure was converted into mae (Maestro, Schrödinger, LLC, New York, NY, USA) format and optimized using OPLS 2005 force field with the default setting (LigPrep, version 3.1, Schrödinger, LLC, New York, NY, 2014.).

Active site predictions
The SVMP modeled protein from our previous work [19] was used in this study (our previous work, three dimensional structure of SVMP was modeled with Zn^{2+} and Ca^{2+} ions. Molecular docking, Prime/MM-GBSA (ΔG_{bind} calculations), Quantum polarized ligand docking (QPLD), QM-MM interaction energy analysis and molecular dynamics simulation were performed for the compound of *Clerodane diterpenoid* with the SVMP in the presence and absence of metal ions (Zn^{2+} and Ca^{2+} The *Clerodane diterpenoid* was significantly inhibited by hemorrhagic activity. The total inhibition of hemorrhagic activity suggested interaction of *Clerodane diterpenoid* with metal/or metalloproteases, neutralizing effects.)). Calcium ion was present in the N- and C- terminal segments in the SVMP protein. The zinc binding environments of the consensus were HEXXHXXGXXHD sequences which contained three histidines (HIS138, HIS142, and HIS148). The active site of SVMP (combinations 1-4) was predicted using the SiteMap in maestro (SiteMap, version 9.8, Schrödinger, LLC, New York, NY, 2014) with default parameters. The possible binding

sites were identified for various physical descriptors such as size, degree of exposure, degree of enclosure, tightness, hydrophilic, hydrogen-bonding possibilities, hydrophobic, and linking site points.

Molecular docking studies
The compounds SID 249494133, SID 249494134, and SID 249494135 were docked into the binding site of all the combinations (combinations 1–4) of SVMP using Glide XP of Glide module (Glide, version 6.4, Schrödinger, LLC, New York, NY, 2014). The shape and properties of the receptors were represented on a grid by several sets of fields that progressively provided more accurate scoring to the ligand poses. For the non polar parts of the receptor, we scaled the van der Waals radii of receptor atoms by 1.00 with a partial atomic charge of 0.25. The grid was generated (12 Å X 12 Å X 12 Å) by specifying the residue as the grid center. The geometric or hydrogen bonding constraints were not introduced for substrate docking. Hydrogen bonding and geometric constraint were not introduced in the substrate docking. The experiments were performed using default parameters.

Quantum polarized ligand docking
SID 249494133, SID 249494134, and SID 249494135 were docked with the improved docking program of QPLD (LigPrep, version 3.1, Schrödinger, LLC, New York, NY, 2014; Glide, version 6.4, Schrödinger, LLC, New York, NY, 2014; Schrödinger Suite 2014-3 QM-Polarized Ligand Docking protocol; Jaguar version 8.5, Schrödinger, LLC, New York, NY, 2014; QSite version 6.4, Schrödinger, LLC, New York, NY, 2014). QPLD was included with QM/MM calculations (Cho *et al.,* 2005[23], Singh and Muthusamy, 2013[24], Kirubakaran *et al.,* 2014)[25]. QPLD docking was carried out in three steps; in the first step, the normal Glide docking with the best ligand poses were acted on. In the second step, the partial charges were replaced on the ligand in the field of receptor for each ligand complex and charges were calculated from the QM calculations. The single point electrostatic calculation was used with 6-31G*/ LACVP* base set and B3LYP density functional theory (DFT). The Ultrafine" SCF accuracy level ($i_{acc} = 1$, $i_{ac\text{-}scf} = 2$) was used for the QM region. In the final step, the ligand was redocked with updated atomic charges with the help

of Glide XP and QPLD and this step returned the most energetically favorable poses.

Prime/MM-GBSA calculations

The docking and QPLD poses were used to calculate the binding free energy using Prime MM-GBSA method. The docked poses were minimized by the local optimization feature in prime. The OPLS-2005 force field was used for calculating the binding free energy for a set of ligands and their receptors. The binding free energy was calculated using the following equation:

$$\Delta G_{Bind} = \Delta E_{MM} + \Delta G_{Solv} + \Delta G_{SA}$$

where ΔE_{MM} is the difference in the minimized energies between the protein-ligand complexes, ΔG_{Solv} is the difference in the GBSA solvation energy of the protein–ligand complex and sum of the solvation energies for the protein and ligand, and ΔG_{SA} is the difference in the surface area energies for the complex and sum of the surface area energies in the protein and ligand. The minimizations of the docked complexes were performed with the local optimization feature of prime.

QM–MM interaction energy calculation

The QM–MM calculations were performed with Glide XP docking of the 249494133, SID 249494134 and SID 249494135 inhibitors and binding to the active site of SVMP for all the combinations (1–4) (QSite version 6.4, Schrödinger, LLC, New York, NY, 2014). The QM–MM interaction energy was investigated using frozen orbital-based and hybrid QM–MM potentials (Murphy *et al.,* 2000)[26] implemented in the Schrödinger Suite (QSite version 6.4, Schrödinger, LLC, New York, NY, 2014). The hybrid potential combines (i) DFT with B3LYP functional to describe the atoms at the active site of SVMP and (ii) includes the molecular mechanics in the effect on protein matrix used for the protein–ligand complex. Single point energy calculations and geometry optimized structures were used with the basis set of LACVP** on the ligand (Tripathi and Singh, 2014)[27]. The geometry optimization of the 6-31G** atoms and OPLS-2005 force field was used with the rest of the system (Jorgensen *et al.,* 1996)[28]. The QM region of all the coordinates was free to adjust during the optimization.

Molecular electrostatic potential calculation

SID 249494133, SID 249494134, and SID 249494135 from the docking study for all the combinations (1-4) were used as input for DFT calculations. The DFT calculations were performed using Jaguar (Jaguar version 8.5, Schrödinger, LLC, New York, NY, 2014). The complete geometry optimization was carried out by hybrid DFT with Becke's three-parameter exchange potential and the Lee-Yang-Parr correlation functional (B3LYP) and 6-31G** basis set level was used. The energy calculations to simulate the physiological conditions were performed in an aqueous environment and using Poisson–Boltzmann solver. Quantum chemical descriptors, MESP, HOMO, LUMO, and solvation energy were carried out by Jaguar. The electrostatic potentials surface was created over the ligand to provide a measure of the electrostatic potential at roughly the van der Waals surface of the molecules. Further, the space extended beyond the molecular surface which provided a measure of charge distribution from the point of view of an approaching reagent. The positive electrostatic potential regions were indicated by the excess positive charge. It was the repulsion of the positively charged test probe. The negative potential regions were indicated by the area of excess negative charge. It was the attraction of the positively charged test probe. 3D isosurfaces of the MESPs at the van der Waals contact surface represent the electrostatic potentials superimposed onto a surface of constant electron density (0.01 e au^{-3}). The color coded isosurface values provide an interaction of the overall molecular size and the location of the positive or negative electrostatic potentials. The deep red and blue colors indicate the most positive and the most negative electrostatic potential regions.

Molecular dynamics simulation

Molecular dynamics (MD) simulation of the protein–ligand complexes for all the combinations (1–4) were carried out using Desmond (Bowers *et al.,* 2006)[29] and OPLS 2005 force field (Kaminski *et al.,* 2001)[30] was used for energy minimization of the system. The protein-ligand complexes were solved in 10 Å X 10 Å X 10 Å cubic boxes with periodic boundary conditions and TIP3 water molecules were solvated. The counter ions (Na$^+$ and Cl$^-$) were

added in the whole system to balance the net charge. In Desmond, equilibration of the whole system was carried out using a default protocol made up of a series of restrained minimizations and MD simulations. The minimized system was relaxed with an NPT (number of atom, pressure, and temperature) ensemble restraining the non-hydrogen solute atom for a 10 ns simulation period. The long-range electrostatic interactions were computed by particle-mesh Ewald method and van der Waals (vdW) cutoff was set to 9 Å. The final confirmation of the protein-ligand complexes was performed by 50 ns of MD simulations. The structural changes and dynamic behavior of the protein were calculated by RMSD.

RESULTS AND DISCUSSION
Active prediction and molecular docking
The active site of SVMP (combinations 1-4) was predicted using the SiteMap in maestro (SiteMap, version 9.8, Schrödinger, LLC, New York, NY, 2014) with default parameters. The molecular docking study was carried out by Glide XP mode of docking (Schrödinger, LLC, New York, NY, 2014). The compounds SID 249494133, SID 249494134, and SID 249494135 were docked into the active site of SVMP. The protein–ligand interactions were separated by four types such as hydrogen bonds, hydrophobic, ionic, and water bridges. The interacted amino acid residues were ZN1, GLY 105, GLU139, GLY105 and ALA164 (combination 1) GLY105, HIS142, LEU166 (combination 2), ZN1, ALA107, GLY105, GLU139, LEU166 (combination 3) and GLU139, LEU166, HIS138 (combination 4) of the SID 249494133. The catalytic zinc-ion is located at bottom of the active-site cleft. Interestingly, due to the presence of ZN ion from the protein, the compounds SID 249494133, SID 249494134, and SID 249494135 interacted with the ion. In addition, HIS142 is a zinc binding residue in the SVMP protein and it functions as a ligand of the catalytic zinc atom in our protein. The catalytic zinc-ion is located at the bottom of the active-site cleft and it is conserved by HIS138, HIS142, and HIS148. The zinc binding environments of the consensus have a well-conserved "HEXXHXXGXXHD" amino acid sequence that harbors the essential catalytic

HIS138, HIS142, and HIS148 triad of the Met-turn. The His138, His142, and His148 were important residues in SVMP protein. This Met-turn surrounds a conserved Met residue that forms a hydrophobic surface that acts as a base for the Zn^{2+}. Calcium ion was identified opposite to the active site of SVMP and close to the crossover point of the N- and C-terminal segments of the M-domain (calcium binding site). The M-domain is close to the calcium binding site and opposes the catalytic zinc atom. Further, the N-terminal and C-terminal domains were bound in the Ca^{2+} ion. This result suggests that zinc ion is essential for the ligand binding and calcium ion is important for the structural integrity of the SVMP. This result clearly shows that HIS142, LEU166, GLU139, and ASP102 are important residues for ligand binding. In addition, the HIS142 is zinc binding residue in this protein and HIS142 functions as a ligand of the catalytic activity. The presence of ions ion from this protein, the carboxyl group was interacted with the protein; in absence of both ions from the protein carboxyl group was not interacted with the protein. The Glide energy score and interacted residues are shown in Tables 1–4. The SID 249494133, SID 249494134, and SID 249494135 docking scores were increased when compare to *Clerodane diterpenoid* (combination 1-4). The docked protein–ligand complexes with hydrogen bond interactions are shown in Supplementary Figure 4-6. Based on the docking study, both the ions (Zn^{2+} and Ca^{2+}) have a significant effect on the ligand binding site.

Quantum polarized ligand docking
The QPLD docking method was used to improve the docking accuracy and for the more accurate treatment of the electrostatic interactions. The QM calculations were derived from the ligand charges in the active site region of the protein. Of the three compounds, SID 249494133 and SID 249494135 have high binding affinities of the QPLD Glide score (Table No.1-4). Due to presence of Zn^{2+} ion in the protein, the QPLD Glide scores had a high binding affinity. The QPLD scores also well correlated with the Glide XP docking results.

Prime/MM-GBSA calculations
MM-GBSA (ΔG_{Bind}) was carried out to calculate the binding free energy of SID 249494133, SID 249494134, and SID 249494135 against SVMP and

to investigate the role of the protein–ligand binding in the active site of SVMP. The results from our energetic analysis of the complexes are shown in Tables No.5-7. The binding free energy calculation of the complexes ~~was~~ obtained by XP docking and QPLD docking strategies. The prime MM/GBSA (ΔG_{Bind}) range (SID 249494135) was -32.567 kcal/mol (combination 1), -50.982 kcal/mol (combination 2), -46.404 kcal/mol (combination 3), and -51.473 kcal/mol (combination 4) (Table 6). SID 249494134 prime MM/GBSA (ΔG_{Bind}) ranged -44.85 kcal/mol (combination 1), -32.627 kcal/mol (combination 2), -20.283 kcal/mol (combination 3) and -38.151 kcal/mol (combination 4) (Table No.5). In SID 249494133 -78.048 kcal/mol (combination 1), -81.838 kcal/mol (combination 2), -63.573 kcal/mol (combination 3) and -76.585 kcal/mol (combination 4) (Table 5). The presence of both the ions in the protein was observed, the ΔG_{Bind} score was increased for all the compounds (Tables No.5-7). In the compound of SID 249494134 the ΔG_{Bind} covalent scores were increased for all the combinations compared with SID 249494133 and SID 249494135. In addition, $\Delta G_{Bindcovalent}$ scores of the three compounds were almost similar for all the combinations. Further, the QPLD Prime MM/GBSA ΔG_{Bind} scores had increased for all the combinations. This result clearly shows that both the ions are required for catalytic activity of the protein (Tables No.8-10). Further, SID 249494135 has a higher binding affinity with SVMP for the four combinations (Tables No.8-10).

QM–MM interaction energy calculation
Molecular electrostatic potential profiles
The stereo electronic complementarities of the ligands and receptors are studied in detail by 3D molecular electrostatic potential (MESP) and other electronic parameters, as these properties mainly drive the molecular recognition in the ligand–receptor interactions. The structural complementarities of the molecules to the receptor were confirmed by docking analysis. Further, in order to understand the surface electronic properties of SID 249494133, SID 249494134, and SID 249494135, we estimated the pharmacophoric features and their complementary surface required for binding. Based on this idea, the molecules were analyzed through MESP, HOMO–LUMO

parameters, and salvation energy. The MESP isosurface of SID 249494133, SID 249494134, and SID 249494135 compounds is superimposed inside the active site of SVMP (Figures No.1-3). The presence of both the electropositive and electronegative portions of SID 249494133, SID 249494134, and SID 249494135 makes this compound more reactive. Three different portions, namely dihydrofuran-2(3H)-one and 2,3-dimethyl cyclohexanol, are mainly involved in the protein–ligand interaction with the key active site residues such as ASP102, HIS142, and LEU166. As mentioned earlier, the presence of ions in the active site plays a vital role in ligand binding.

Highest occupied and lowest unoccupied molecular orbitals
The orbital energies of HOMO and LUMO were also calculated (Tables No.11-13). In the protein–ligand binding, systematically, the electron acceptor ability of LUMO plays a crucial role compared with the electron donor property of HOMO. The HOMO eigenvalues of the molecules were more negative, which indicates higher HOMO energies and thus stable binding of electrons to the nuclei. The more negative values of LUMO indicate the lower LUMO energy and a strong affinity for electrons. The stability of the molecules was also confirmed by the calculated energy gap between HOMO and LUMO. HOMO–LUMO gap is an acute parameter to determine the molecular admittance. Consequently, the largest HLG value indicates a more stable molecule and the rearrangement of its electron density (Cao *et al.,* 2003)[31]. The HOMO and LUMO energies are small, ranging between -0.23 and 0.21 (SID 249494133), -0.24 and 0.26 (SID 249494134) and -0.37 and 0.31 (SID 249494135). Because of the small values of HOMO and LUMO, both hasty electron transfer and exchange are evenly possible, and the creation of these molecules is very reactive. In SID 249494134, the HOMO and LUMO were plotted on the carboxyl group of the compound (Figures No.5 and 8) and this group was interacted with zinc atom. HOMO and LUMO maps were visualized as p-like orbitals for the possible molecular interaction analysis (Cao *et al.,* 2003)[31]. In the presence and absence of ions, the HOMO and LUMO sites are plotted onto the molecular surface of the

compounds as shown in Figures No.4-6 (HOMO) and Figures No.7-9 (LUMO). The reactive features and the substituent influence on the electronic structure of the compounds were characterized by these quantum chemical calculations results. Due to the presence of both the ions in the protein, the HOMO was plotted more on the carboxyl group of SID 249494135. In addition, the combination 3 LUMO was plotted more on the carboxyl group of SID 249494134.

Molecular dynamics simulation of protein–ligand complexes

MD simulation study was performed to check the stability and dynamic properties of the protein–ligand complexes. The simulations were carried out by four environmental conditions for the combinations 1-4. The dynamic stability of the complexes was assessed during the MD simulation and RMSDs of the backbone are plotted in Figures No.10-12 (SID 249494133). The RMSD of SID 249494133 (combinations 2 and 3) is more fluctuating from 0 to 10 ns (Figure 10) compared with combinations 1 and 4. The combination 4 (SID 249494134) backbone RMSDs of the protein was more stable in the simulation period of 10 ns (Figure No.11). In combination 4, the RMSD (SID 249494135) is more fluctuating from 6 to 10 ns and combination 3 is more stable during the simulation period of 10 ns (Figure No.12). In SID 249494134 (combination 3), it is less fluctuating at 9Å from 6 to 10 ns and combination 4 is less fluctuating at 6 ns compared with combinations 1 and 2 (Figure No.11). The RMSD reached the maximum deviation it could because of the absence of Zn^{2+} ion in the protein.

Protein secondary structure

The protein secondary structure results are shown in Figures No.13-15. The alpha helical conformations were more conserved in the simulation period of 10 ns. In SID 249494133 and SID 249494135 (combination 2 and 4) was observed small amounts of alpha helix loss at 0–10 ns (Figure). Particularly, the absence of Zn^{2+} ion from the protein alpha helix was lost. In SID 249494134 (combination 4), it is also observed that a small amount of alpha helix was lost during the simulation period of 10 ns (Figure No.14).

Protein–ligand contacts

SID 249494133 had a consistent ionic bond interaction (combination 1) with HIS138, GLU139, HIS142, and HIS148 up to 10 ns. In addition, SID 249494134 and SID 249494135 also had an ionic bond network with HIS138, GLU139, HIS142, and HIS148 (combination 1). Interestingly, these compounds are capable of the formation of ionic-mediated bridges with zinc atom (Figures No.16A, 17A, and 18A).

In combination 2, the intermolecular hydrogen bonds were THR103, ILE104, GLY105, HIS125, GLU139, ASN147, HIS148, SER163, and LEU166 (SID 249494133, SID 249494134 and SID 249494135) (Figures No.16B, 17B, and 18B).

In combination 3, the amino acid residues were THR103, HIS139, ALA164 (SID 249494133), HIS125 (SID 249494134), LYS117, ASN147, and HIS148 (SID 249494135) during the simulation period of 10 ns (Figures 16C, 17C and 18C). At 10 ns of MD simulation, the hydrogen bond interaction of the residues HIS138, GLU139, and HIS148 had more stability. SID 249494134 had greater ionic bond interaction compared with SID 249494133 and SID 249494134.

Combination 4 had more number of H-bonds interacted through MD simulation for SID 249494133, SID 249494134, and SID 249494135. The residues were ASP101, ASP102, THR103, ALA107, TYR108, LYS116, LYS117, HIS138, GLU139, HIS142, ASN147 and HIS148 throughout the MD simulation. The number of interactions increased due to the absence of Zn^{2+} ion in the complex (Figures No.16D, 17D, and 18D).

These three compounds formed stable hydrogen bond interactions with the protein for the four combinations. More hydrophobic interactions were interacted with protein because of the absence of Zn^{2+} ion. These three compounds were stabilized by more ionic bond interaction with HIS138, GLU139, HIS142, and HIS148 in the simulation period of 10 ns. The compounds of SID 249494133, SID 249494133, and SID 249494133 show good interaction with the critical active site residues of HIS138, GLU139, HIS142, and HIS148.

Table No.1: Combinations 1-4 analyzed by docking simulations studies and their corresponding Glide scores, Glide energy and hydrogen bond interactions

S.No		Ions	Glide XP docking			QPLD docking		
			Glide score (kcal/mol)	Glide energy (kcal/mol)	H-bond interactions	Glide score (kcal/mol)	Glide energy (kcal/mol)	H-bond interactions
1	SID 249494133	Combination 1	-6.370	-41.225	ZN1, LEU166 GLU139, GLY 105, ALA164	-7.017	-54.09	ZN1, LEU166, GLU139, GLY 105, ALA 164
2		Combination 2	-8.774	-47.160	GLY105, HIS142, LEU166	-9.339	49.798	LEU166, GLU139
3		Combination 3	-5.931	-50.977	ZN1, ALA107, GLY105, GLU139, LEU166	-7.694	-60.39	ASP102, GLU139, THR103
4		Combination 4	-8.470	-40.876	GLU139, LEU166, HIS138	-5.833	-47.642	LEU166, GLU139

Table No.2: Combinations 1-4 analyzed by docking simulations studies and their corresponding Glide scores, Glide energy and hydrogen bond interactions

S.No		Ions	Glide XP docking			QPLD docking		
			Glide score (kcal/mol)	Glide energy (kcal/mol)	H-bond interactions	Glide score (kcal/mol)	Glide energy (kcal/mol)	H-bond interactions
1	SID 249494134	Combination 1	5.099	-32.883	ZN1, LEU166	-5.939	-37.743	ZN1, LEU166
2		Combination 2	-2.879	-9.370	LYS117, VAL109, ASP102	-3.187	-23.325	ALA164
3		Combination 3	-5.088	-24.194	ZN1, ASP102	-5.978	-39.326	ZN1, HIE125
4		Combination 4	-2.757	-16.227	LEU166	-3.154	-23.856	ALA164

Table No.3: Combinations 1-4 analyzed by docking simulations studies and their corresponding Glide scores, Glide energy and hydrogen bond interactions

S.No		Ions	Glide XP docking			QPLD docking		
			Glide score (kcal/mol)	Glide energy (kcal/mol)	H-bond interactions	Glide score (kcal/mol)	Glide energy (kcal/mol)	H-bond interactions
1	SID 249494135	Combination 1	-8.596	-40.680	ZN1, LEU166, GLU168, ASP102, ASP101	-8.596	-47.948	ZN1, GLU168, ASP 101, ASP 102, LEU166, ALA 164
2		Combination 2	-10.046	-38.628	ALA164, LEU166, GLU139, HIS138, HIS125	-5.505	-45.198	ASP102, GLY105, GLU139, THR103, LYS117
3		Combination 3	-8.636	-33.633	ZN1, HIS148, ALA107, LYS117	-7.316	-41.206	ZN1, ASP102, LYS117, VAL109
4		Combination 4	-8.867	-38.950	ASP102, THR103, GLU139, HIS138, VAL109, LYS117, GLY105	-10.776	-51.42	ASP102, GLY105, HIS138, GLH139, ALA164, LYS117

Table No.4: Combinations 1-4 analyzed by docking simulations studies and their corresponding Glide scores, Glide energy and hydrogen bond interactions (*Clerodane diterpenoid*)

S.No	Ions	Glide XP docking				QPLD docking		
		Glide score (kcal/mol)	Glide energy (kcal/mol)	H-bond interactions		Glide score (kcal/mol)	Glide energy (kcal/mol)	H-bond interactions
1	Combination 1	-2.66	-27.56	ZN1		-4.21	-37.22	ZN1, VAL109
2	Combination 2	-4.27	-29.79	HIS142, ILU166		-5.09	-34.98	HIS142, ILU166
3	Combination 3	-3.44	-25.53	ILU166, ASP102		-3.93	-29.15	ILU166, ASP102
4	Combination 4	-4.18	-31.14	HIS142		-4.96	-37.79	HIS142, ILU166

Table No.5: Binding free energy results for the combinations 1-4 (Docking)

S.No		Ions	ΔG_{Bind} Hbond (kcal/mol)	ΔG_{Bind} Coulomb (kcal/mol)	ΔG_{Bind} Covalent (kcal/mol)	ΔG_{Bind} Lipo (kcal/mol)	ΔG_{Bind} (kcal/mol)	ΔG_{Bind} SolvGB (kcal/mol)	ΔG_{Bind} vdW (kcal/mol)
1	SID 249494134	Combination 1	-2.095	-41.341	8.389	-48.545	-78.048	44.043	-38.499
2		Combination 2	-0.977	-30.115	3.484	-49.149	-81.838	35.369	-40.45
3		Combination 3	-1.71	-26.189	14.877	-50.918	-63.573	42.321	-42.873
4		Combination 4	-0.974	-26.097	9.346	-55.439	-76.585	37.042	-40.462

Table No.6: Binding free energy results for the combinations 1-4 (Docking)

S.No	SID 249494134	Ions	ΔG_{Bind} Hbond (kcal/mol)	ΔG_{Bind} Coulomb (kcal/mol)	ΔG_{Bind} Covalent (kcal/mol)	ΔG_{Bind} Lipo (kcal/mol)	ΔG_{Bind} (kcal/mol)	ΔG_{Bind} SolvGB (kcal/mol)	ΔG_{Bind} vdW (kcal/mol)
1		Combination 1	-0.119	19.567	6.04	-38.559	-44.85	-12.569	-19.213
2		Combination 2	-0.243	81.134	19.467	-40.894	-32.627	-58.309	-0.276
3		Combination 3	-0.249	64.038	4.954	-26.82	-20.283	-42.997	-19.209
4		Combination 4	-0.214	34.732	5.814	-13.329	-38.151	-13.904	-21.251

Table No.7: Binding free energy results for the combinations 1-4 (Docking)

S.No	SID 249494135	Ions	ΔG_{Bind} Hbond (kcal/mol)	ΔG_{Bind} Coulomb (kcal/mol)	ΔG_{Bind} Covalent (kcal/mol)	ΔG_{Bind} Lipo (kcal/mol)	ΔG_{Bind} (kcal/mol)	ΔG_{Bind} SolvGB (kcal/mol)	ΔG_{Bind} vdW (kcal/mol)
1		Combination 1	-1.664	81.795	4.191	-20.198	-32.567	-67.494	-29.197
2		Combination 2	-1.503	115.881	4.551	-29.304	-50.982	-109.984	-30.622
3		Combination 3	-4.759	69.916	4.19	-22.471	-46.404	-70.875	-22.405
4		Combination 4	-4.784	88.355	7.666	-32.173	-51.473	-77.866	-32.671

Table No.8: Binding free energy results for the combinations 1-4 (QPLD)

S.No	SID 249494135	Ions	ΔG_{Bind} Hbond (kcal/mol)	ΔG_{Bind} Coulomb (kcal/mol)	ΔG_{Bind} Covalent (kcal/mol)	ΔG_{Bind} Lipo (kcal/mol)	ΔG_{Bind} (kcal/mol)	ΔG_{Bind} SolvGB (kcal/mol)	ΔG_{Bind} vdW (kcal/mol)
1		Combination 1	-2.256	-41.629	11.707	-47.973	-75.799	43.934	-42.499
2		Combination 2	-2.130	-29.658	3.933	-22.191	-49.574	41.672	-41.200
3		Combination 3	3.450	22.432	5.43	34.943	57.944	37.854	38.985
4		Combination 4	0.851	-19.338	5.94	-50.777	-75.105	33.638	-43.170

Table No.9: Binding free energy results for the combinations 1-4 (QPLD)

S.No	SID 249494135	Ions	ΔG_{Bind} Hbond (kcal/mol)	ΔG_{Bind} Coulomb (kcal/mol)	ΔG_{Bind} Covalent (kcal/mol)	ΔG_{Bind} Lipo (kcal/mol)	ΔG_{Bind} (kcal/mol)	ΔG_{Bind} SolvGB (kcal/mol)	ΔG_{Bind} vdW (kcal/mol)
1		Combination 1	-0.119	20.16	6.059	-39.495	-44.666	11.938	-22.853
2		Combination 2	-0.539	88.031	4.784	-11.047	-3.959	65.609	-19.579
3		Combination 3	-0.122	28.850	5.556	-38.426	-44.398	21.116	-19.140
4		Combination 4	-0.243	61.310	6.010	-26.670	-19.593	41.223	-19.284

Table No.10: Binding free energy results for the combinations 1-4 (QPLD)

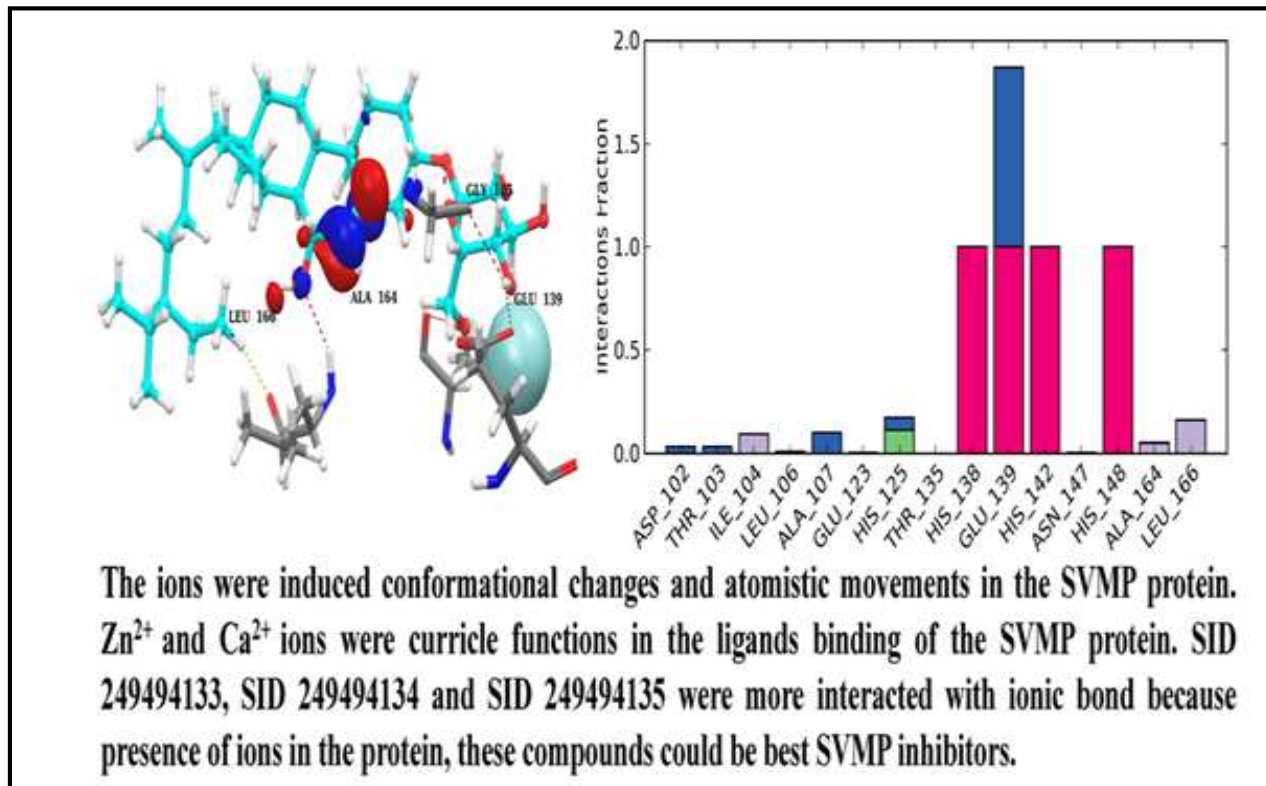| S.No	SID 249494135	Ions	ΔG_{Bind} Hbond (kcal/mol)	ΔG_{Bind} Coulomb (kcal/mol)	ΔG_{Bind} Covalent (kcal/mol)	ΔG_{Bind} Lipo (kcal/mol)	ΔG_{Bind} (kcal/mol)	ΔG_{Bind} SolvGB (kcal/mol)	ΔG_{Bind} vdW (kcal/mol)
1		Combination 1	-1.664	81.795	4.191	-20.198	-32.567	67.494	-29.197
2		Combination 2	3.593	73.933	7.032	14.943	32.098	43.345	36.098
3		Combination 3	-4.056	78.724	10.106	-27.987	-34.404	25.629	-65.563
4		Combination 4	-4.793	120.335	8.034	-11.702	-28.466	109.817	-30.523

Table No.11: Calculated by HOMO and LUMO gaps of SID 249494133

S.No	SID 249494135	Ions	QM–MM energy (kcal/mol)	HOMO (eV)	LUMO (eV)	HLG (eV)
1		Combination 1	-1915.9254	0.025	0.210	-0.185
2		Combination 2	-1915.3652	0.067	0.315	-0.248
3		Combination 3	-1915.5870	0.010	0.230	-0.22
4		Combination 4	-1915.1234	0.038	0.251	-0.213

Table No.12: Calculated by HOMO and LUMO gaps of SID 249494134

S.No	SID 249494135	Ions	QM–MM energy (kcal/mol)	HOMO (eV)	LUMO (eV)	HLG (eV)
1		Combination 1	-1415.817	0.094	0.315	-0.221
2		Combination 2	-1415.634	0.063	0.340	0.277
3		Combination 3	1416.306	0.077	0.310	-0.233
4		Combination 4	1415.808	0.171	0.346	0.175

Table No.13: Calculated by HOMO and LUMO gaps of SID 249494135

S.No	SID 249494135	Ions	QM–MM energy (kcal/mol)	HOMO (eV)	LUMO (eV)	HLG (eV)
1		Combination 1	-2861.8468	0.158	0.302	-0.144
2		Combination 2	-2860.9617	0.216	0.353	-0.137
3		Combination 3	-2861.7525	0.082	0.089	-0.007
4		Combination 4	-2861.1253	0.192	0.315	-0.123

Graphical Abstract

The ions were induced conformational changes and atomistic movements in the SVMP protein. Zn^{2+} and Ca^{2+} ions were curricle functions in the ligands binding of the SVMP protein. SID 249494133, SID 249494134 and SID 249494135 were more interacted with ionic bond because presence of ions in the protein, these compounds could be best SVMP inhibitors.
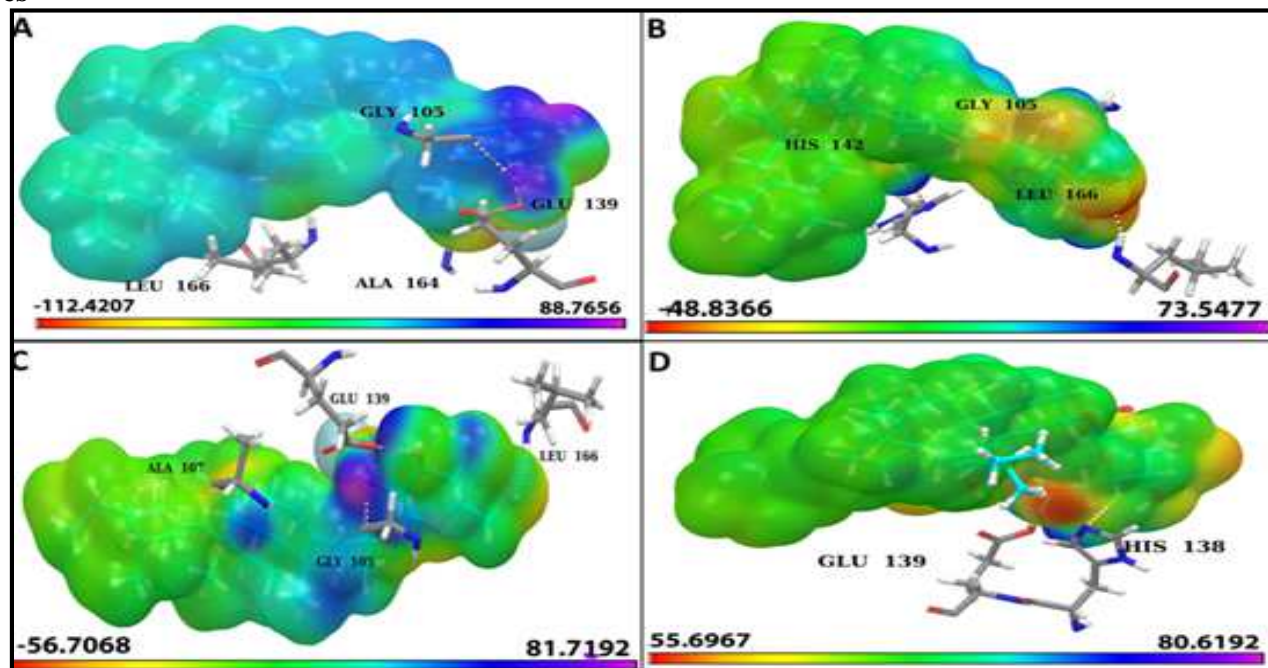
Figures

Figure No.1. The compound of the SID 249494133 MESP superimposed onto a surface of constant electron density for combination 1-4. Showing the most positive potential region (deepest blue color) and most negative potential regions (deepest red color) in the active site of SVMP
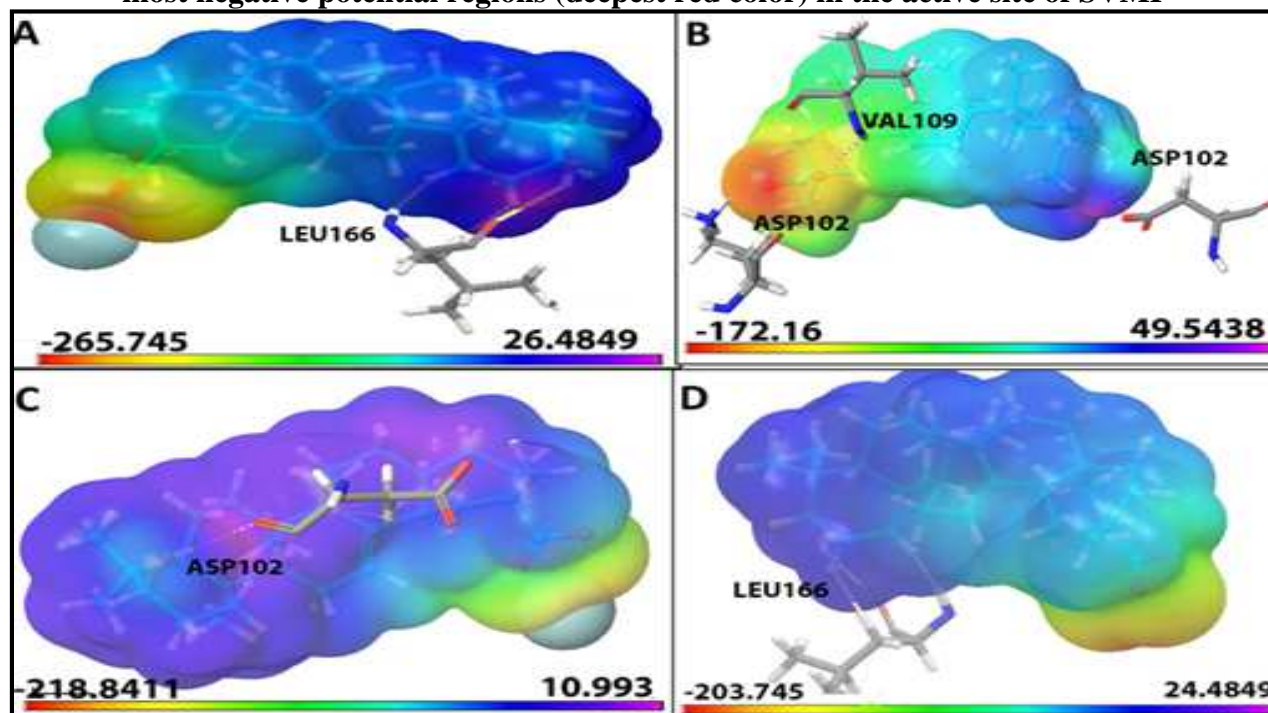
Figure No.2: The compound of the SID 249494134 MESP superimposed onto a surface of constant electron density for combination 1-4. Showing the most positive potential region (deepest blue color) and most negative potential regions (deepest red color) in the active site of SVMP
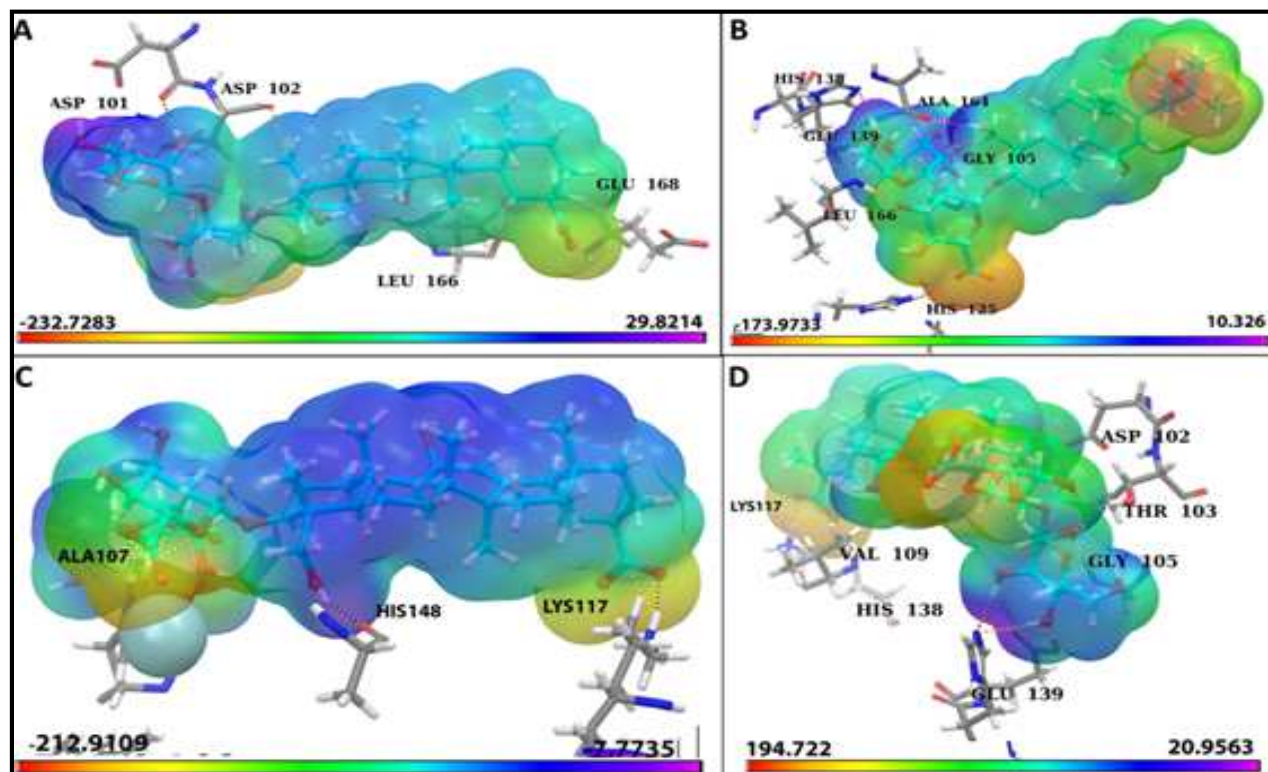
Figure No.3: The compound of the SID 249494135 MESP superimposed onto a surface of constant electron density for combination 1-4. Showing the most positive potential region (deepest blue color) and most negative potential regions (deepest red color) in the active site of SVMP
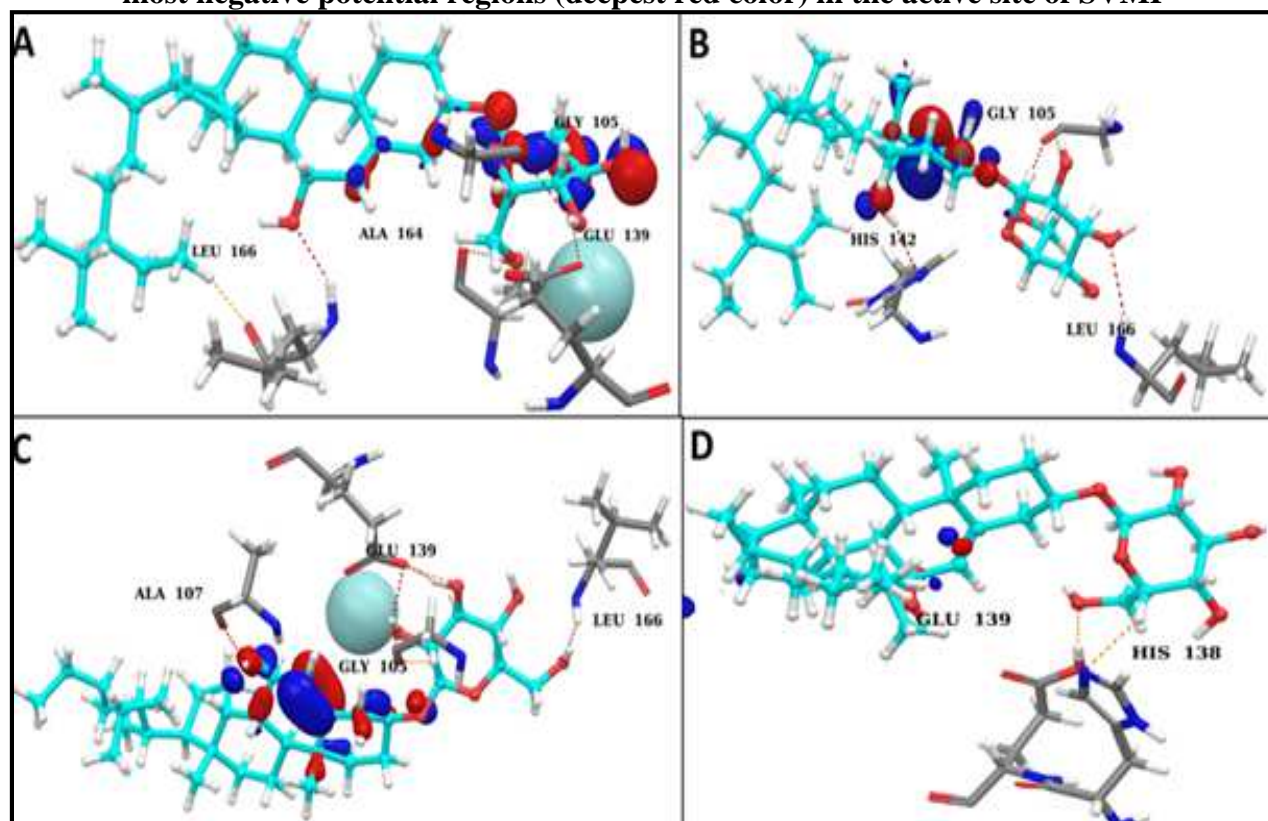
Figure No.4: Plots of the highest occupied molecular orbital of combinations 1-4 (SID 249494133)
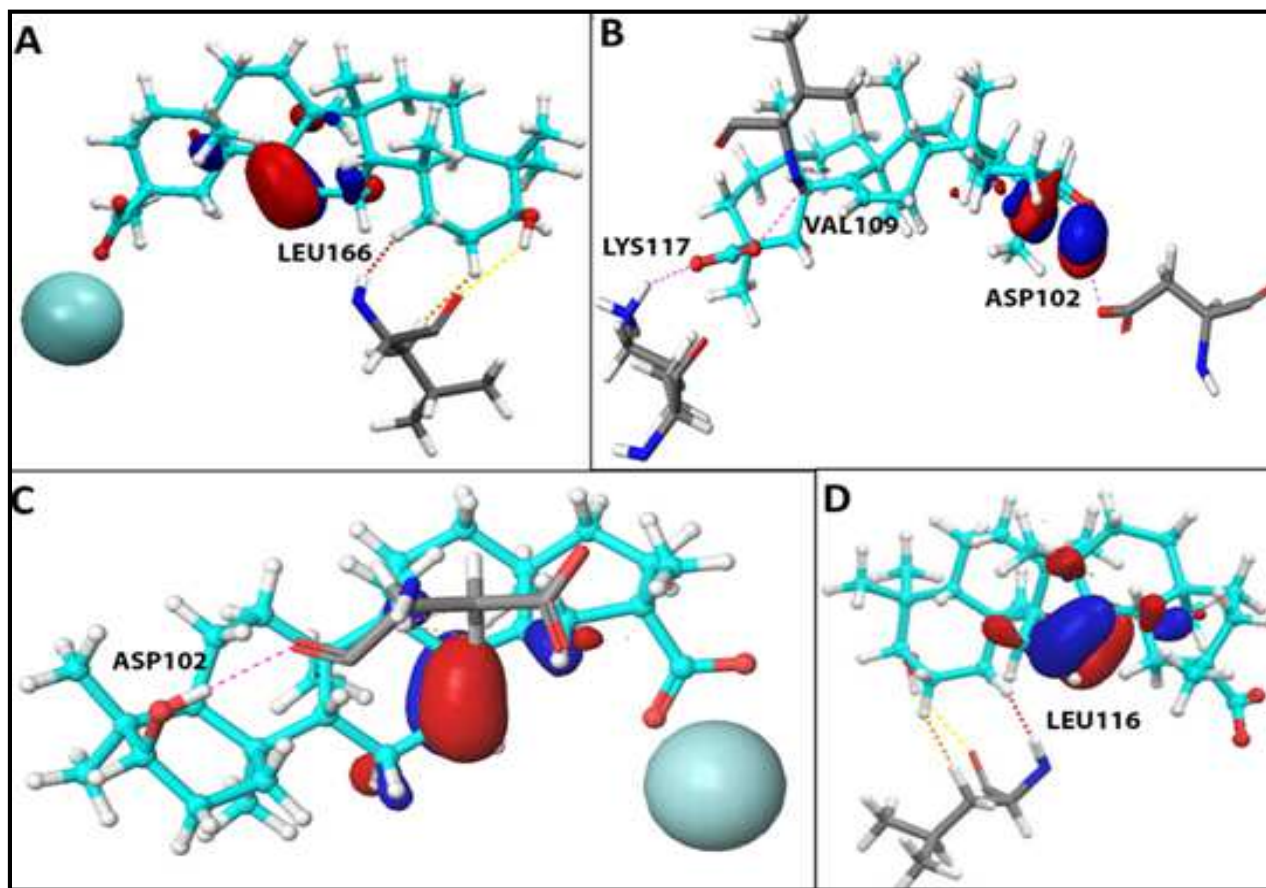
Figure No.5: Plots of the highest occupied molecular orbital of combinations 1-4 (SID 249494134)
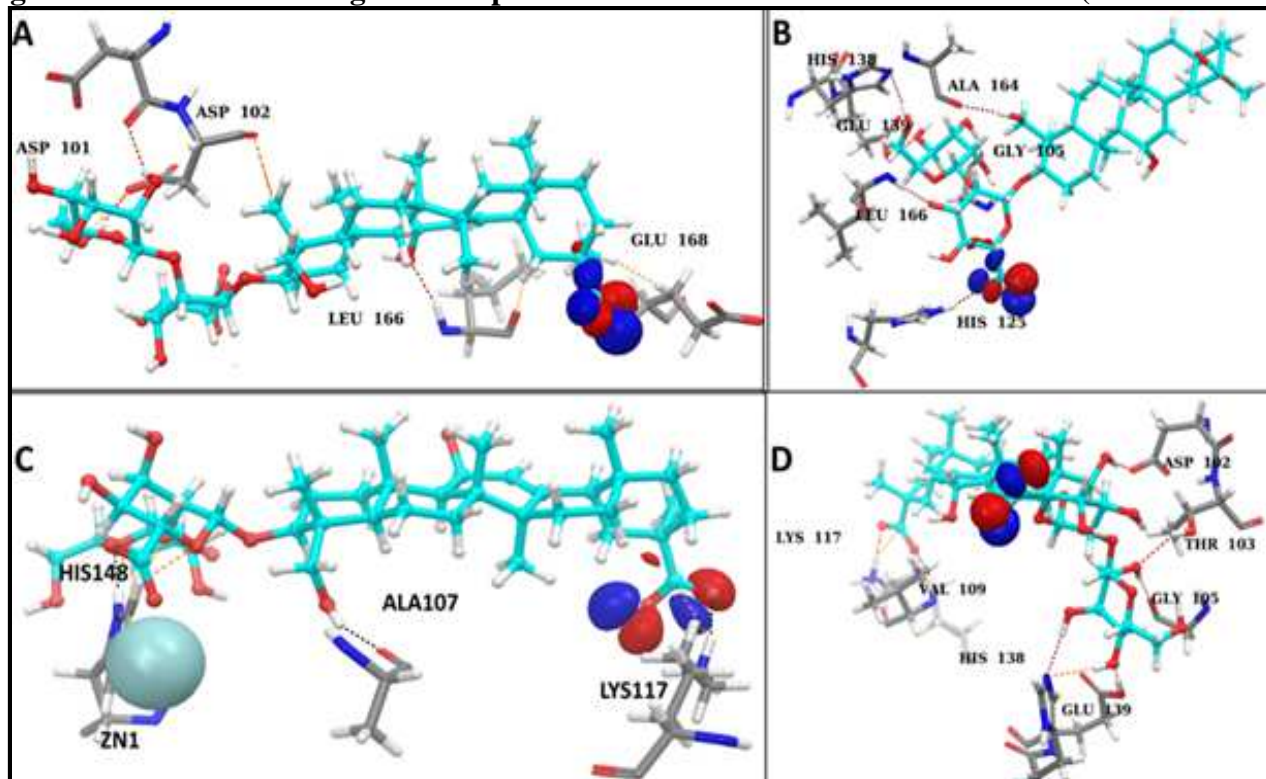
Figure No.6: Plots of the highest occupied molecular orbital of combinations 1-4 (SID 249494135)
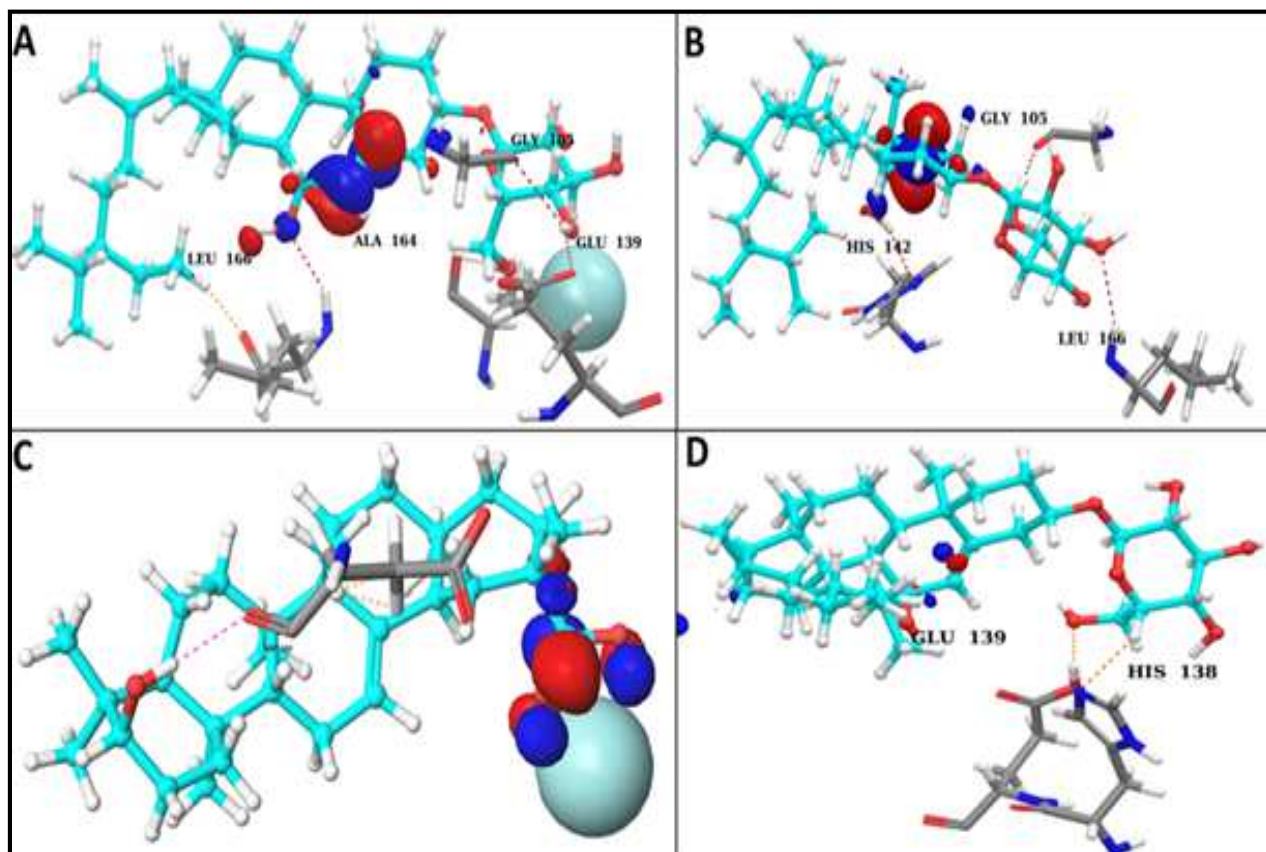
Figure No.7: Plots of the lowest unoccupied molecular orbital of combinations 1-4 (SID 249494133)
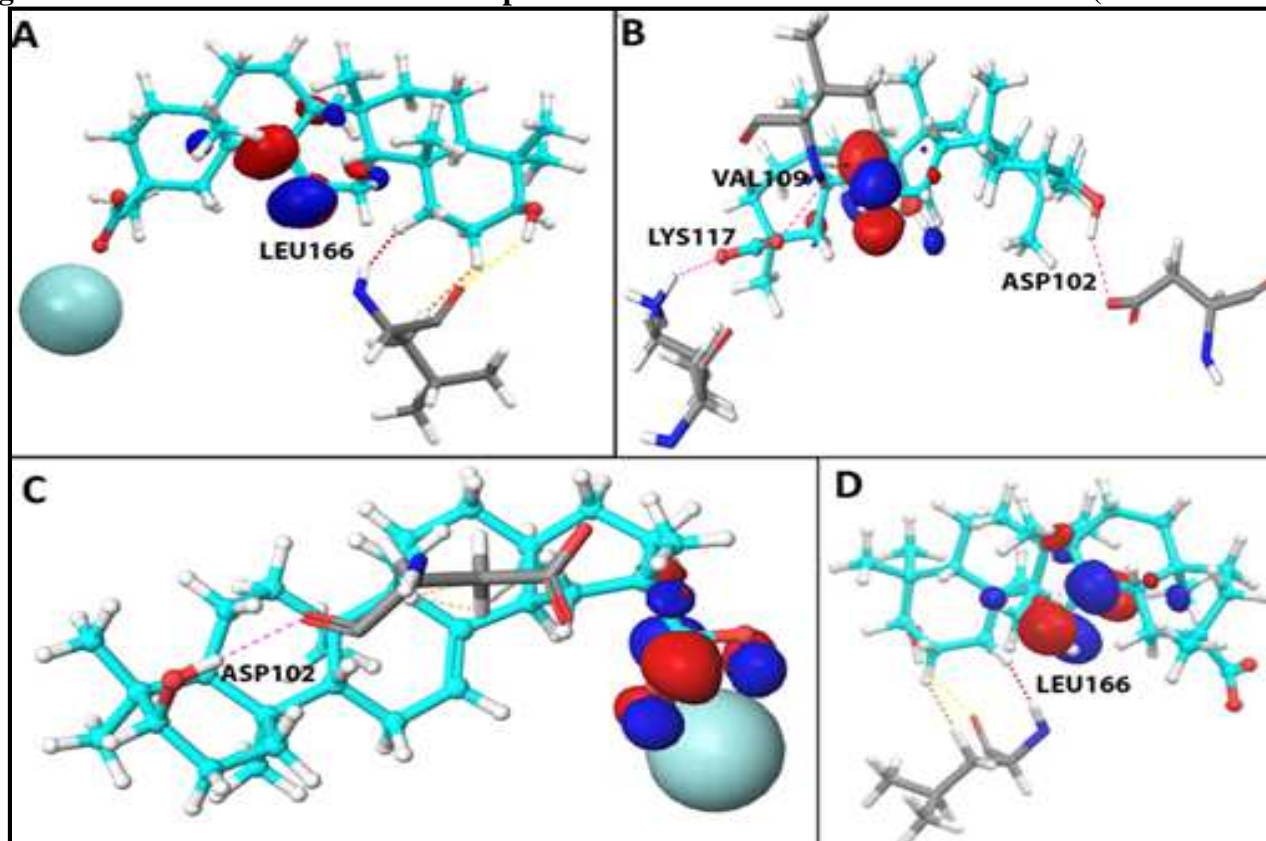
Figure No.8: Plots of the lowest unoccupied molecular orbital of combinations 1-4 (SID 249494134)
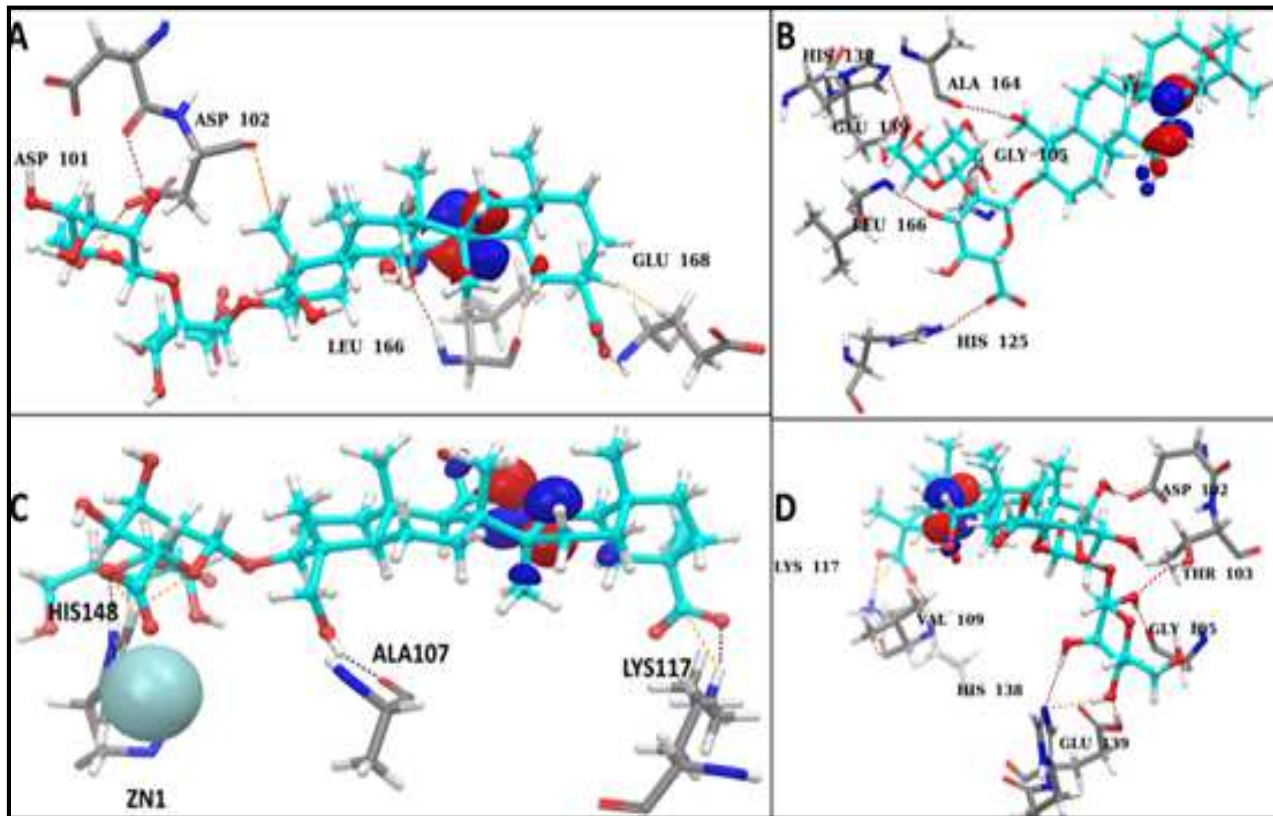
Figure No.9: Plots of the lowest unoccupied molecular orbital of combinations 1-4 (SID 249494134)
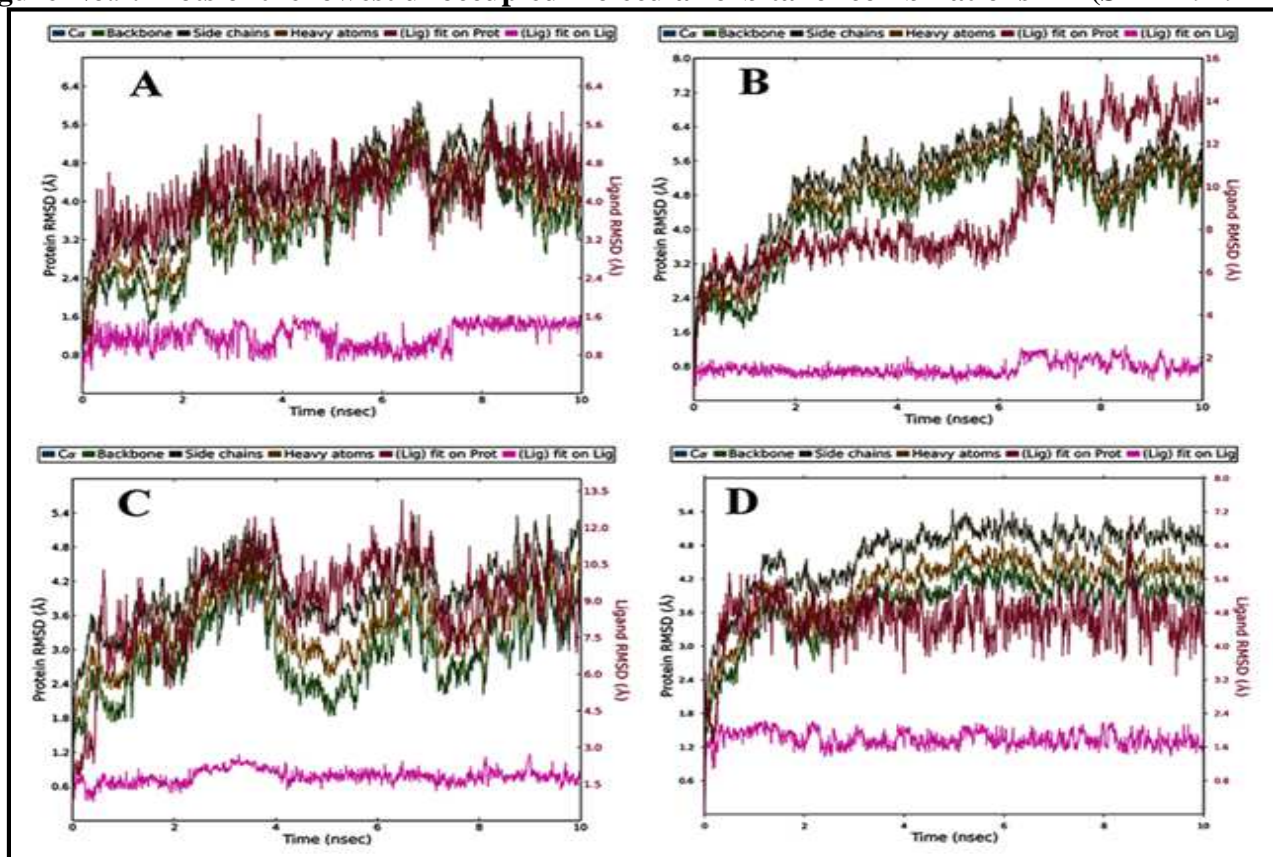
Figure No.10: The backbone RMSD of the protein and SID 249494133 the whole simulation time
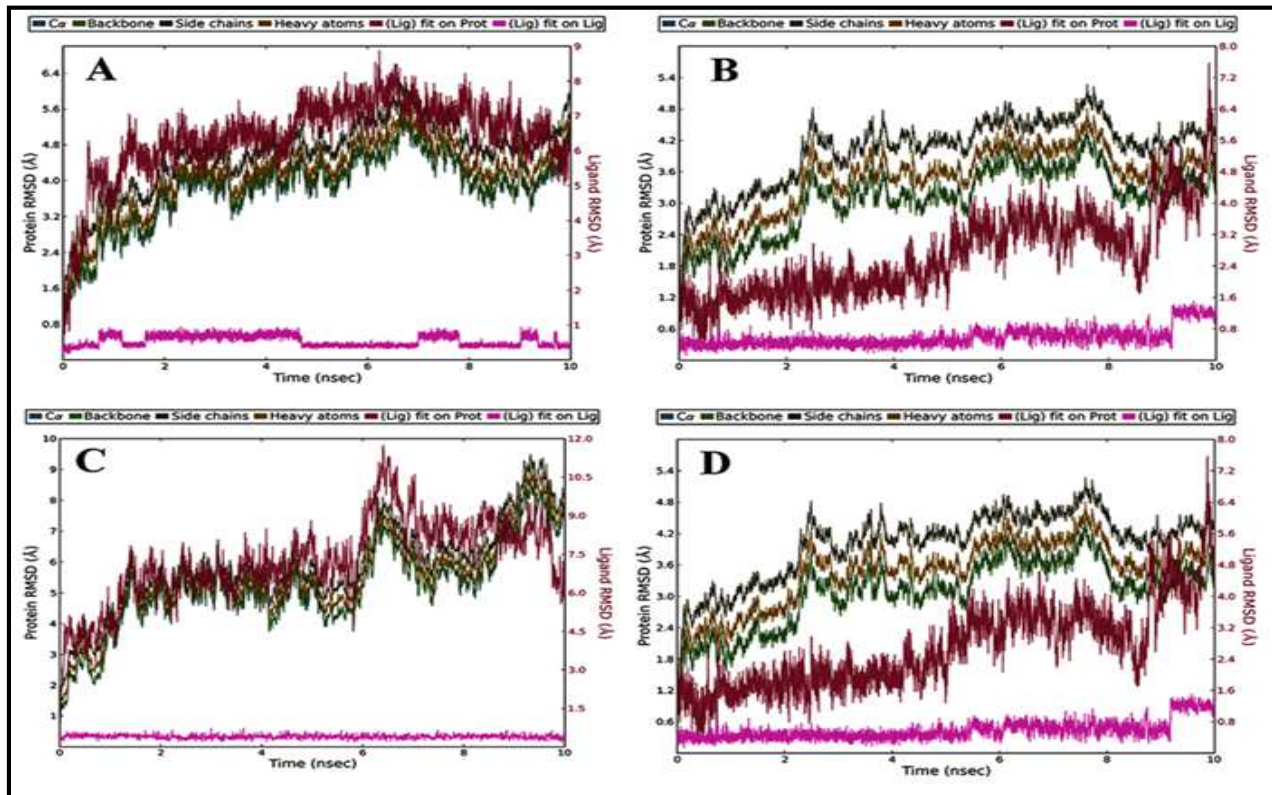
Figure No.11: The backbone RMSD of the protein and SID 249494134 the whole simulation time
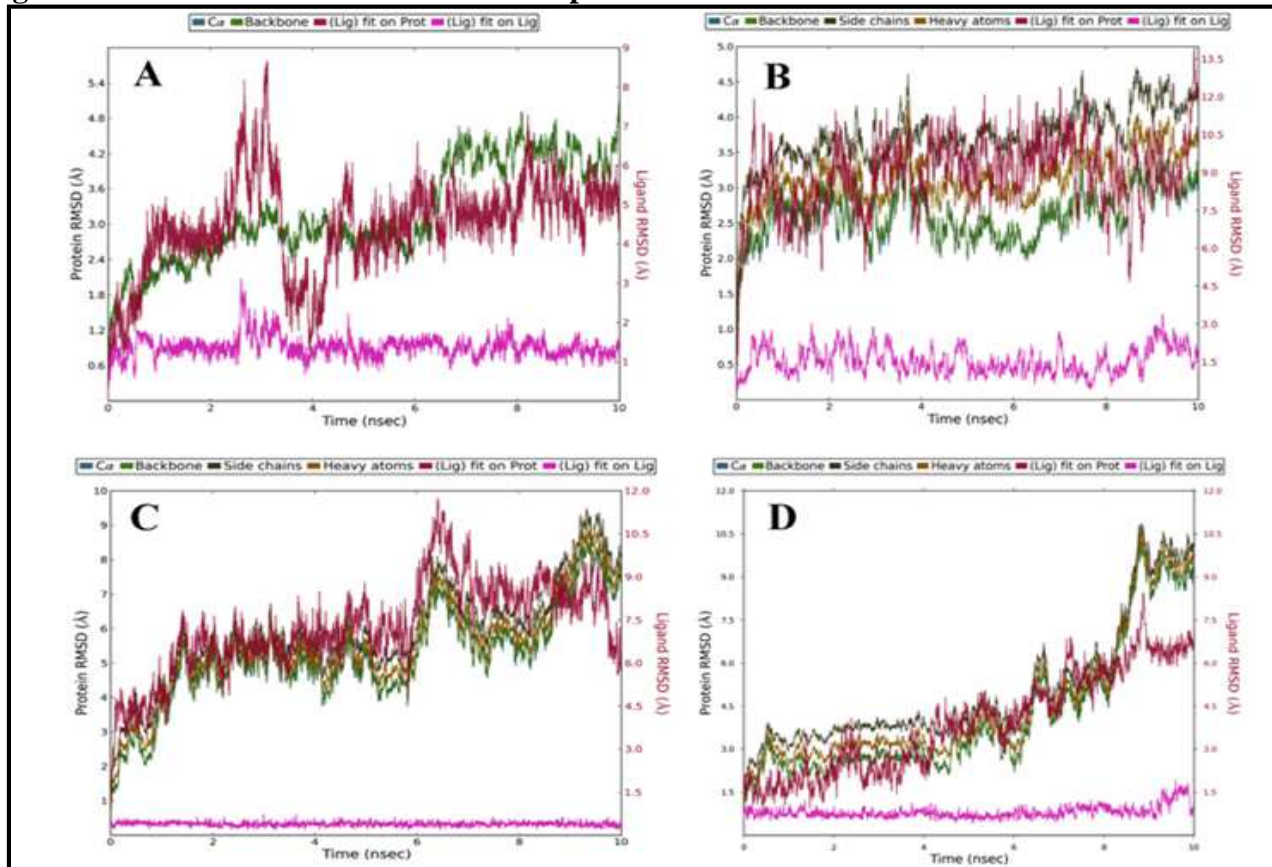
Figure No.12: The backbone RMSD of the protein and SID 249494135 the whole simulation time
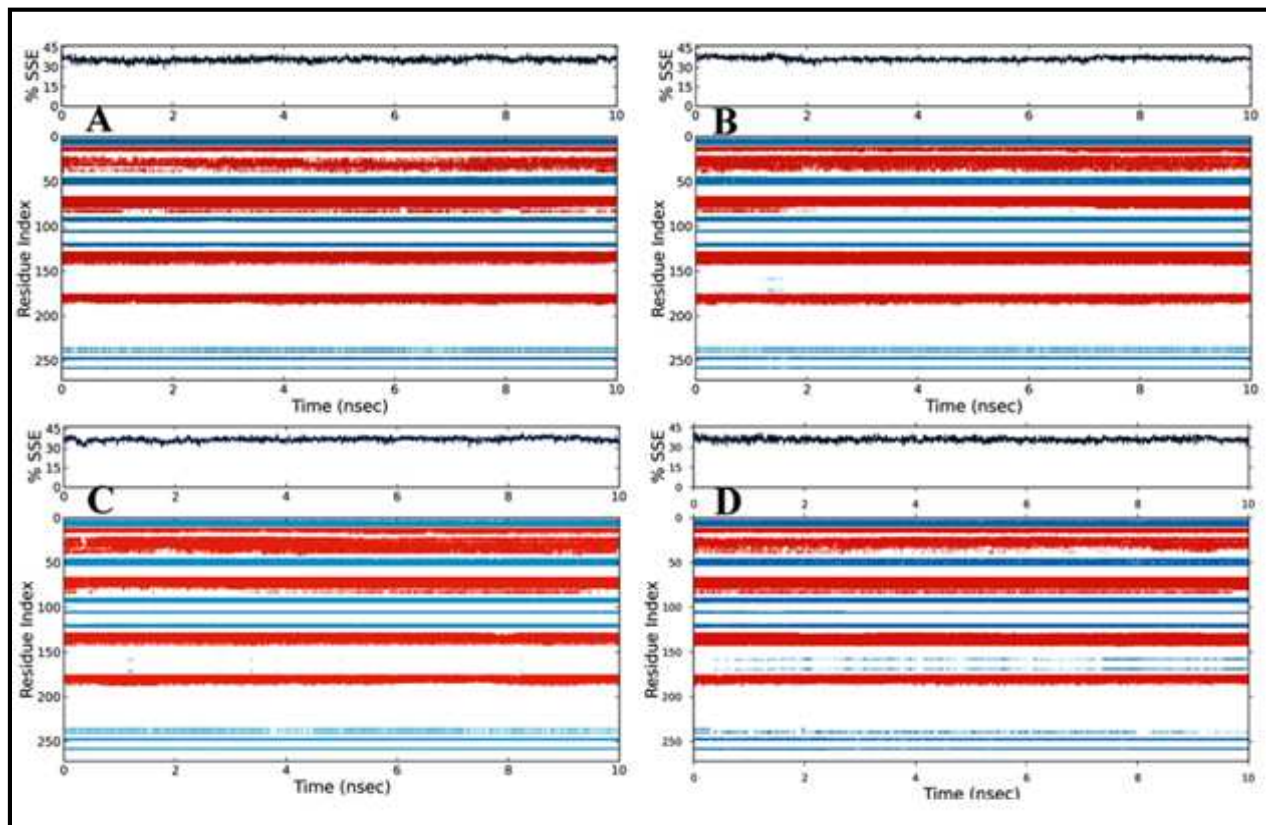
Figure No.13: The evaluation of the secondary structure of combinations 1–4 (SID 249494133)
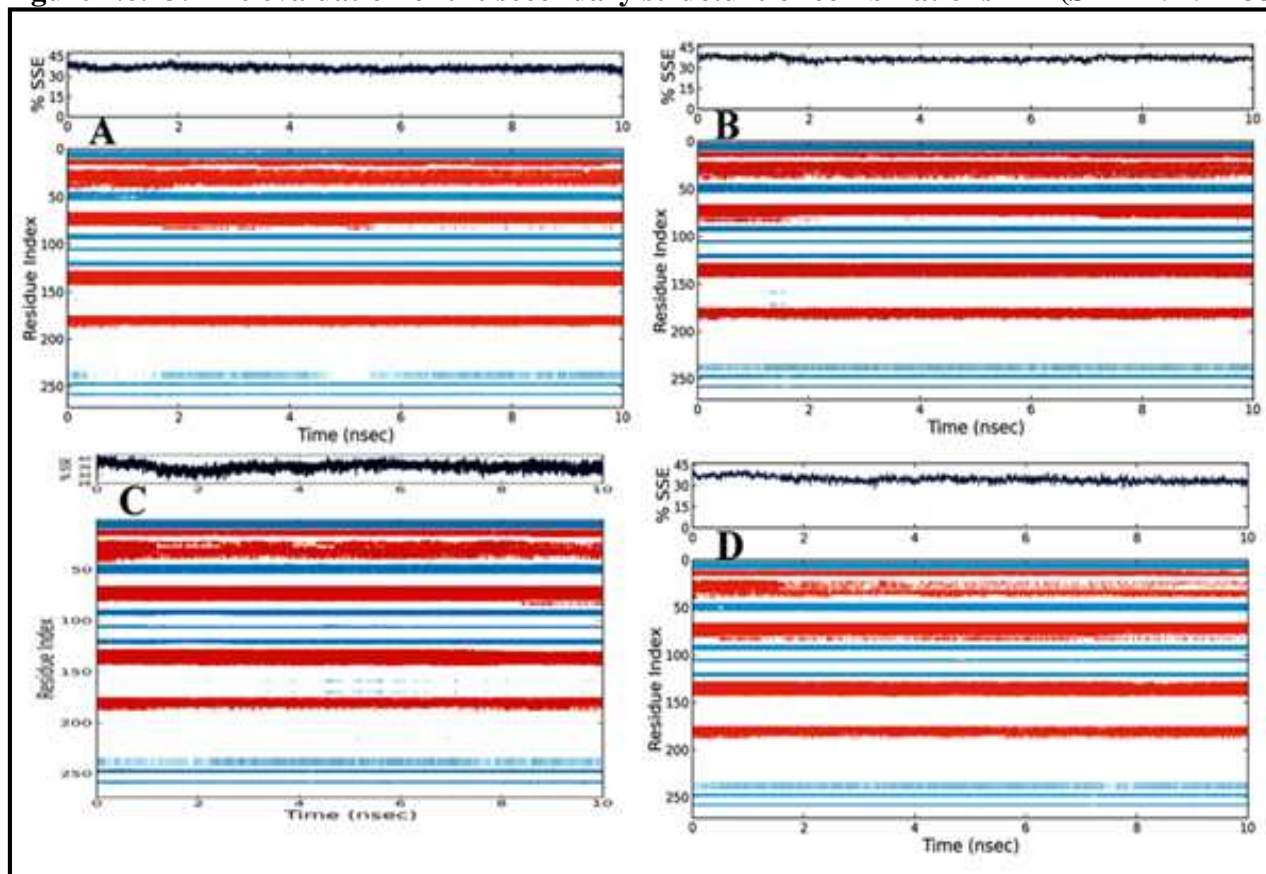
Figure No.14: The evaluation of the secondary structure of combinations 1–4 (SID 249494134)
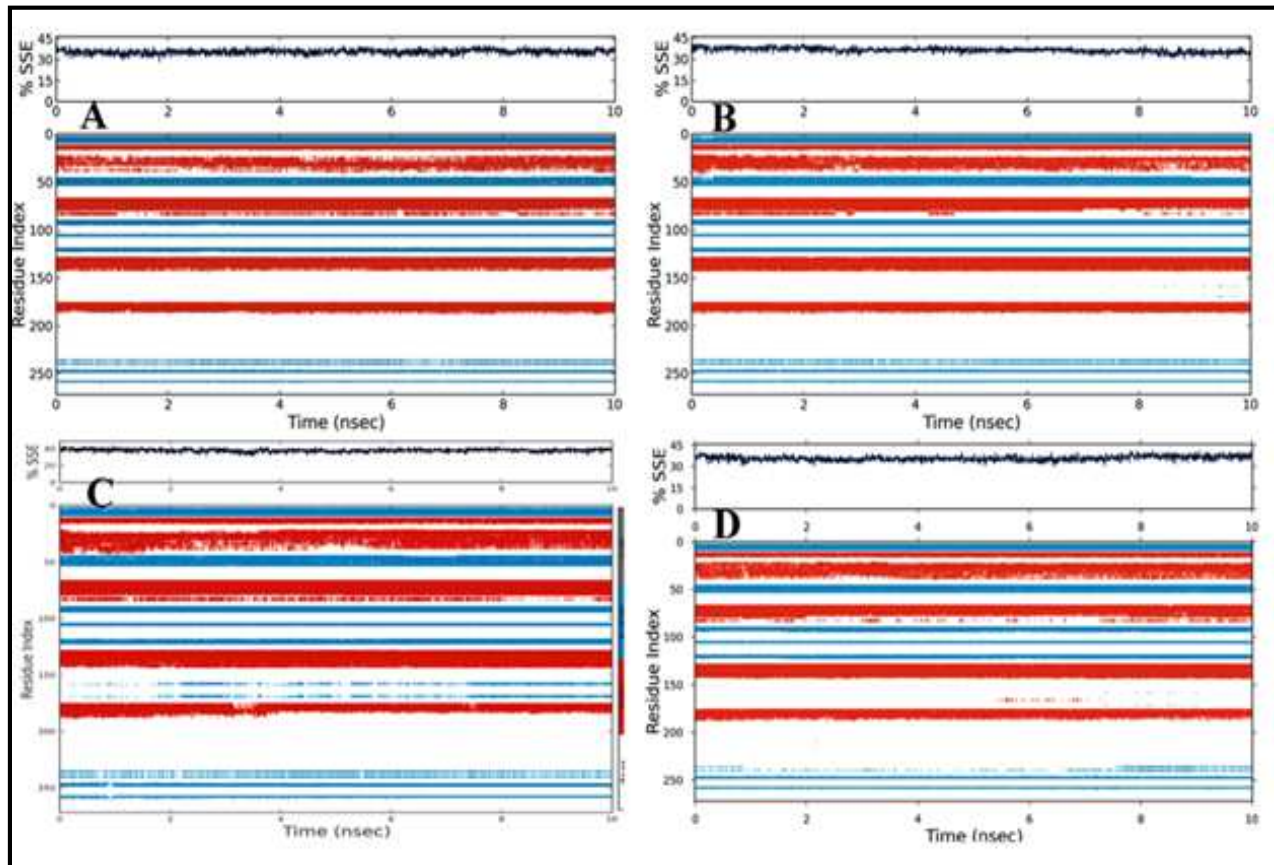
Figure No.15: The evaluation of the secondary structure of combinations 1–4 (SID 249494135)
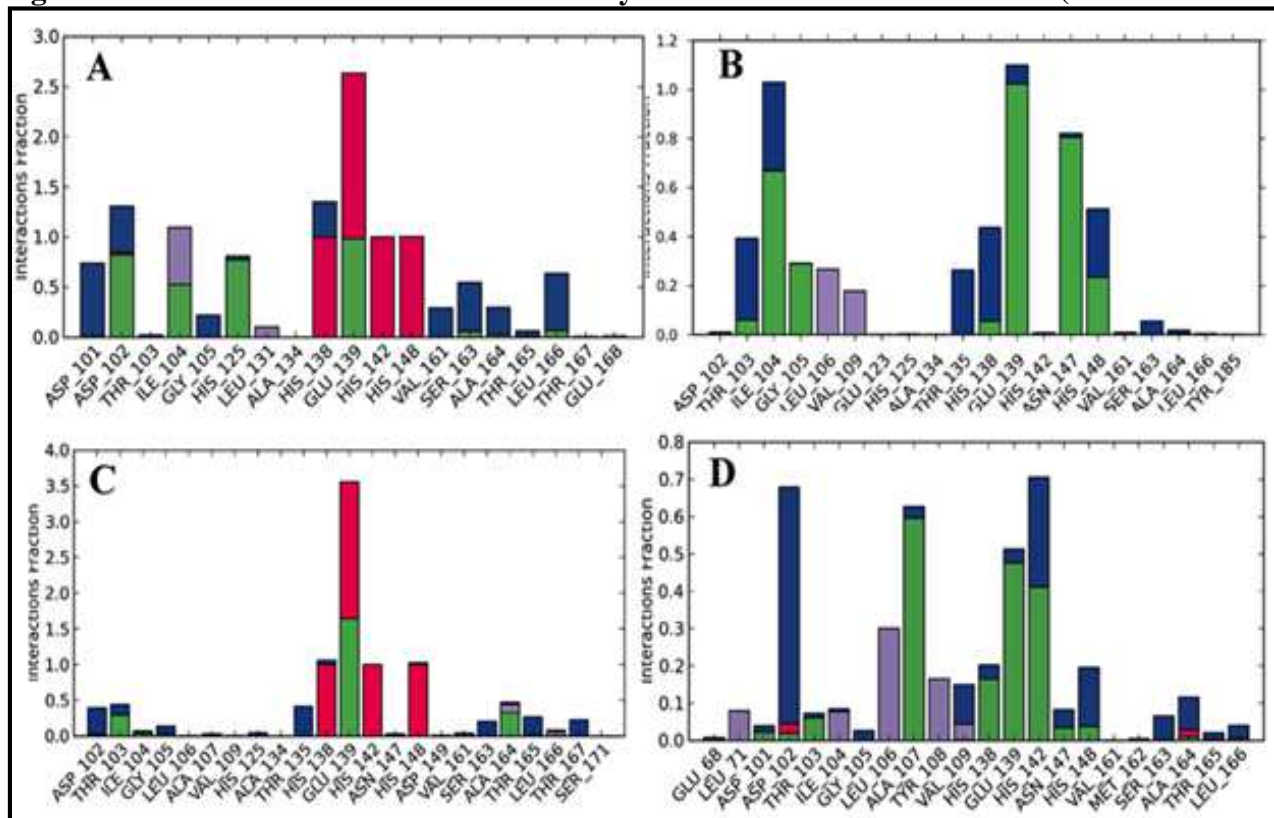
Figure No.16: Protein–ligand contacts through 10 ns simulation (combinations 1–4) (SID 249494133)
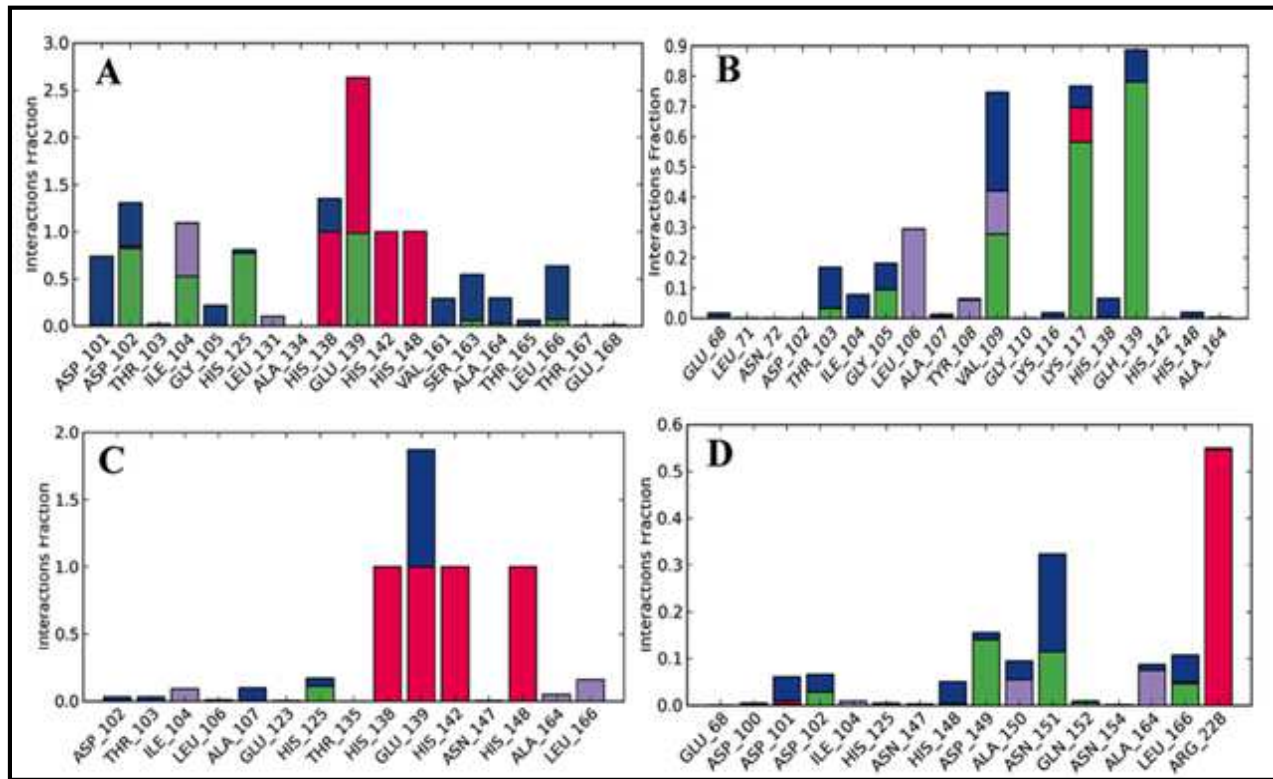
Figure No.17: Protein–ligand contacts through 10 ns simulation (combinations 1–4) (SID 249494134)
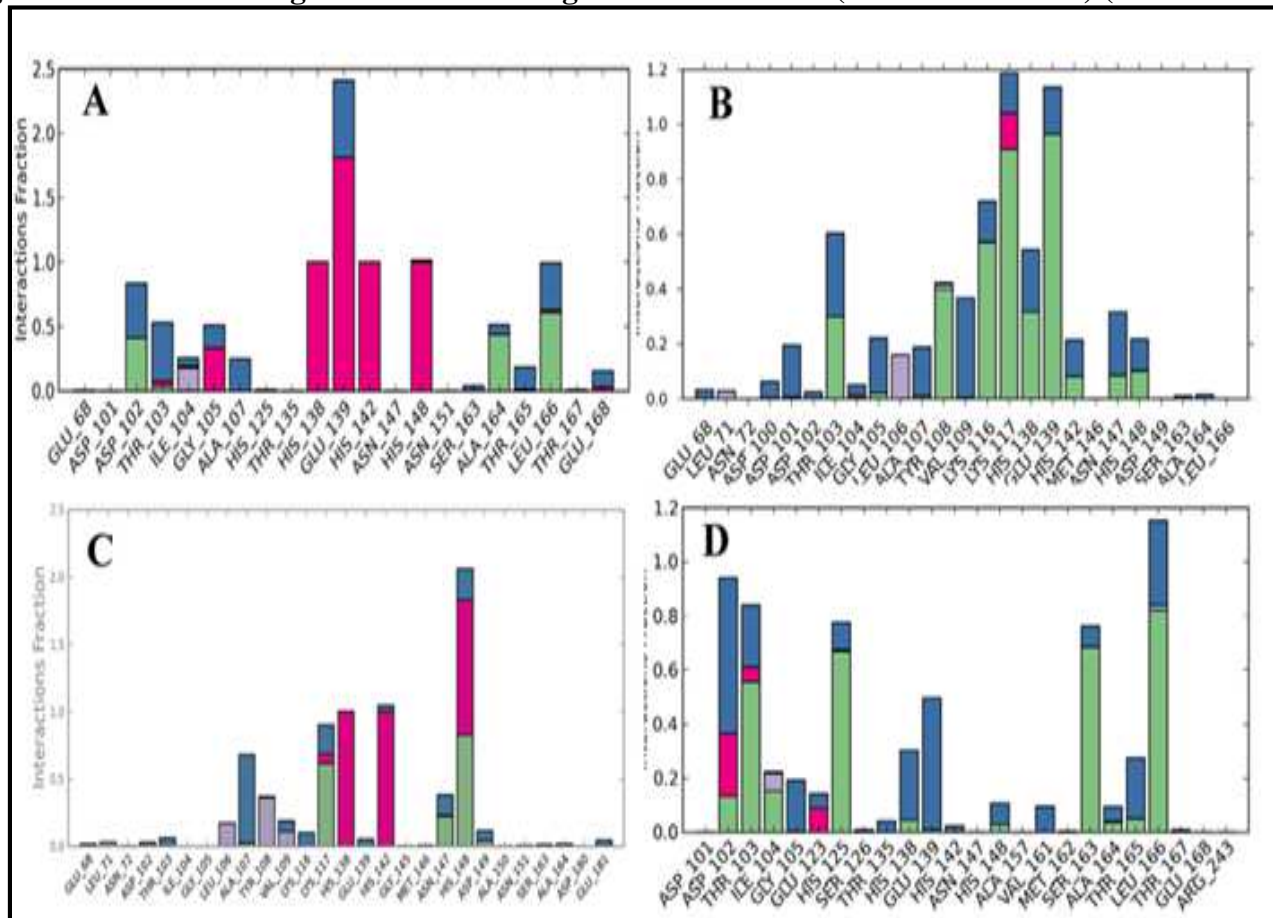
Figure No.18: Protein–ligand contacts through 10 ns simulation (combinations 1–4) (SID 249494135)
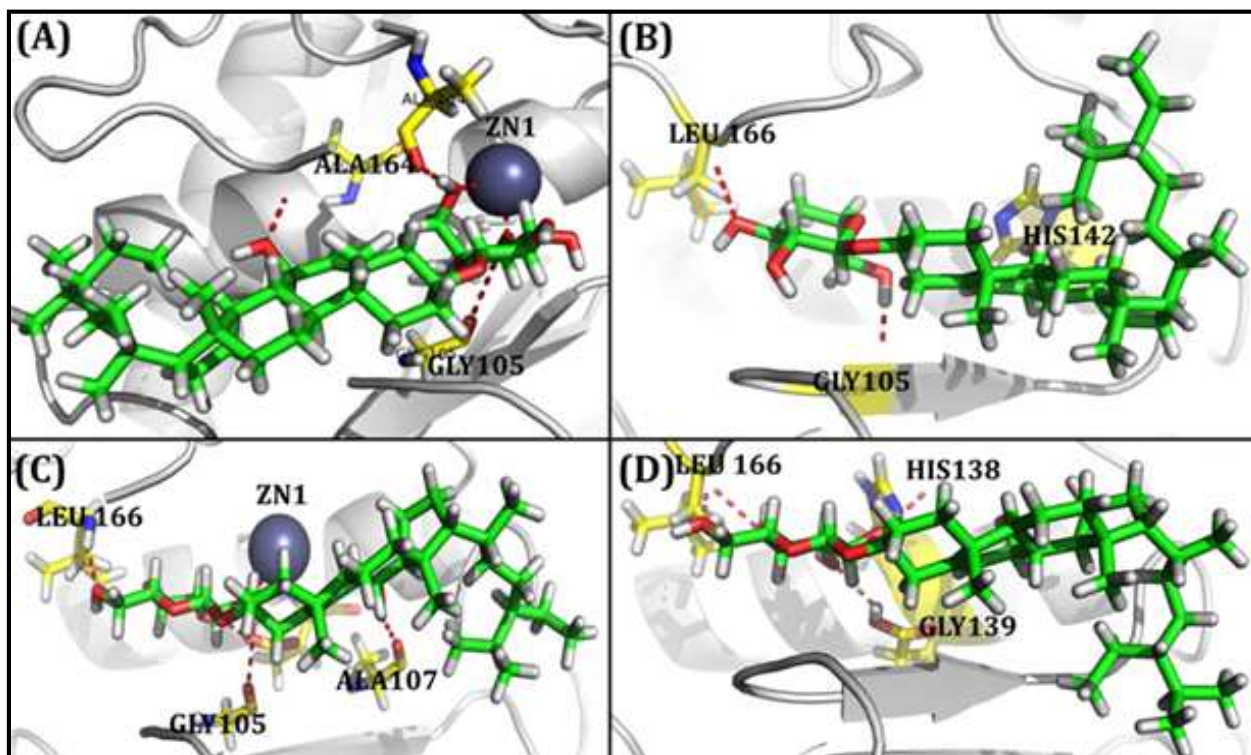
Supplementary Figure
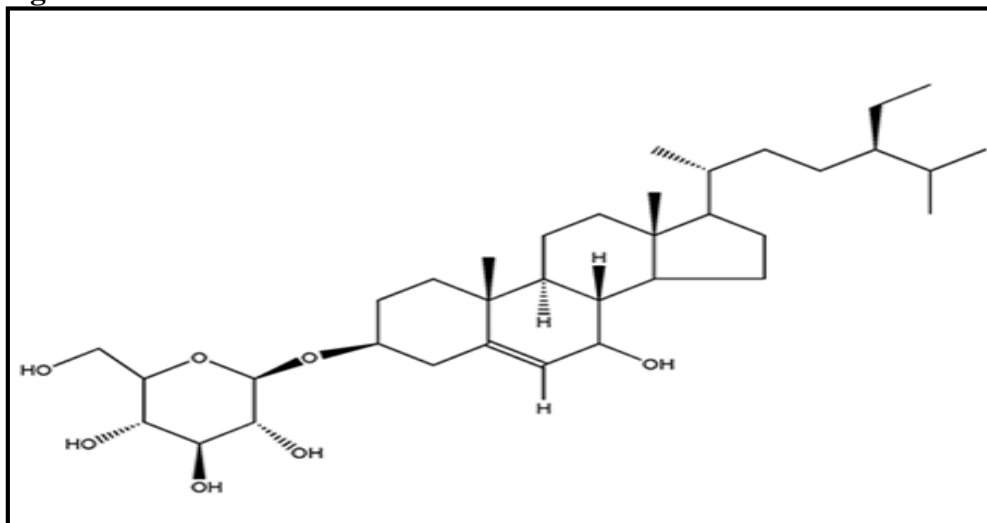
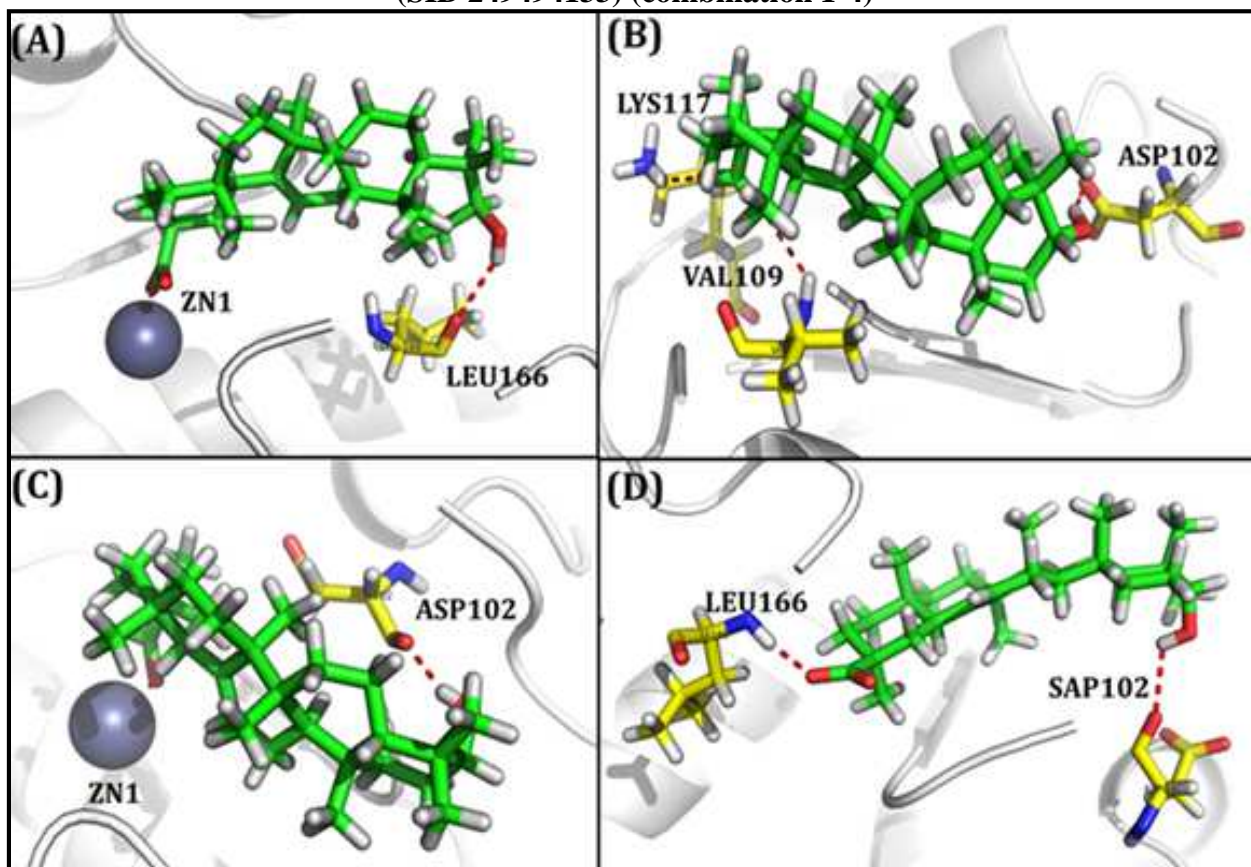**Supplementary Figure No.1: The isolated compound of SID 249494133**
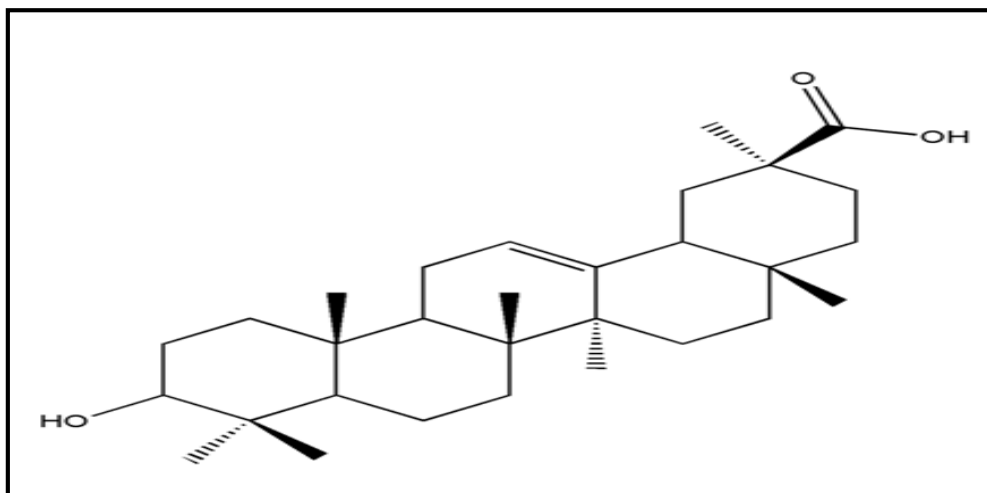
Supplementary Figure No.2: The isolated compound of SID 249494134
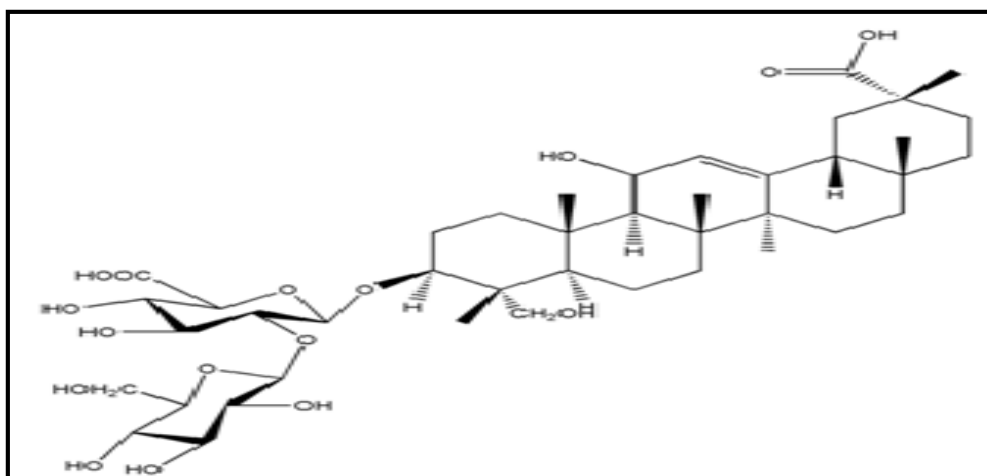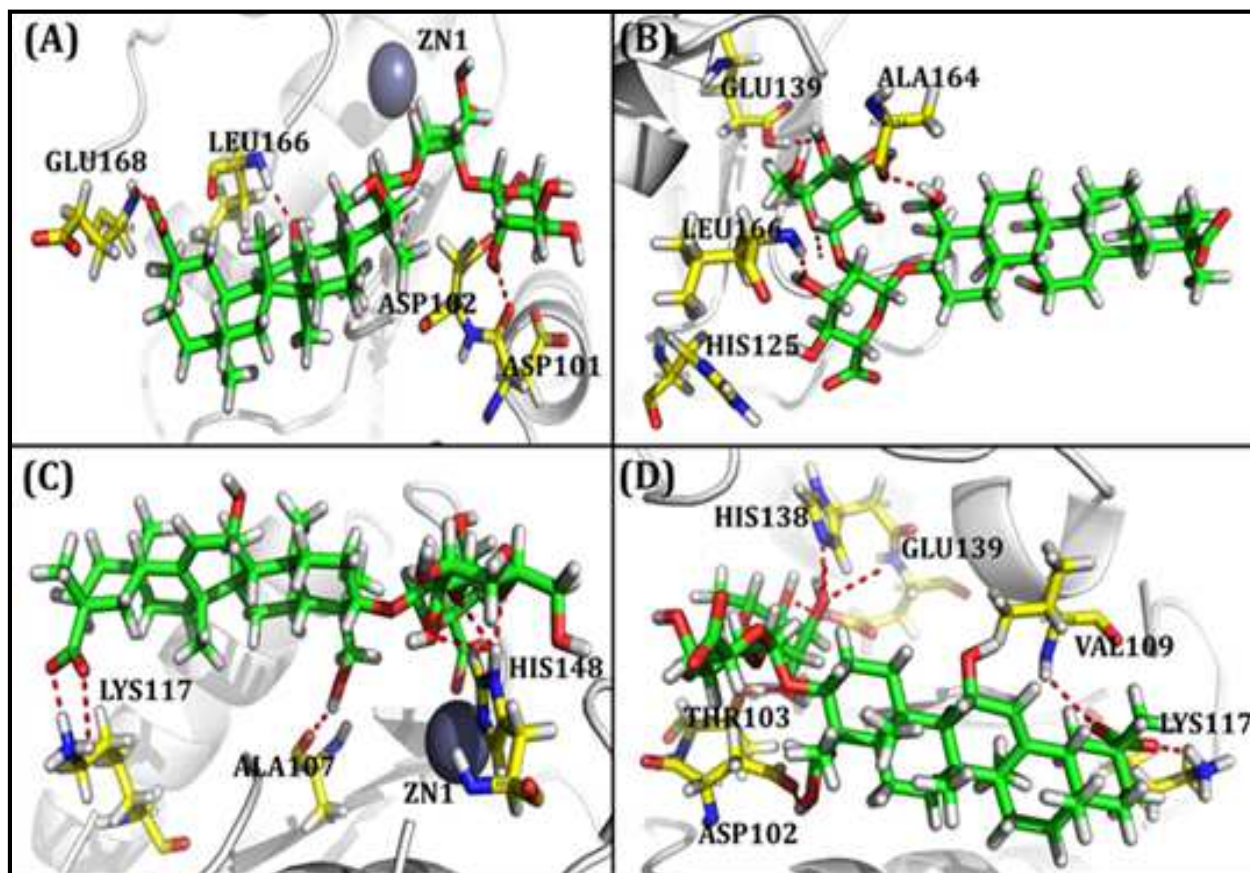

Supplementary Figure No.3: The isolated compound of SID 249494135

Supplementary Figure No.4: The docked protein–ligand complexes with hydrogen bond interactions (SID 249494133) (combination 1-4)

Supplementary Figure No.5: The docked protein–ligand complexes with hydrogen bond interactions (SID 249494134) (combination 1-4)

Supplementary Figure No.6: The docked protein–ligand complexes with hydrogen bond interactions SID 249494135) (combination 1-4)

CONCLUSION

In summary, the docking, QPLD, binding free energy calculation and MD simulation results shows that Zn^{2+} ion present in this active site of SVMP has a vital function. The results show that HIS138, GLU139, HIS142, and HIS148 are crucial residues in the active site of SVMP. All the compounds SID 249494133, SID 249494134, and SID 249494135 were well interacted with the ionic bond network (Zn^{2+} ion) of the protein. These three compounds can demonstrate to be highly effective if included into drug development phases and experimental studies. These three compounds might have inhibitory effect against the SVMP protein. Based on these results, we have concluded that zinc ion is essential for the ligand binding and calcium ion is important for the structural integrity of the SVMP. Furthermore, the SID 249494133, SID 249494134, and SID 249494135 could be potent inhibitors of the SVMP protein compare to *Clerodane diterpenoid*.

ACKNOWLEDGEMENT

CONFLICT OF INTEREST

We declare that we have no conflict of interest.

BIBLIOGRAPHY

1. Fox J W. Serrano, S M. Timeline of key events in snake venom metalloproteinase research, *J Proteomics,* 72(2), 2009, 200-209.
2. Laraba-Djebari Fatima and Chérifi Fatah. Pathophysiological and Pharmacological Effects of Snake Venom Components: Molecular Targets, *Toxicol,* 4(2), 2014, 2-9.
3. Ramos O H, Selistre-de-Araujo H S. Snake venom metalloproteases-structure and function of catalytic and disintegrin domains,

Comp Biochem Physiol C ToxicolPharmacol, 142(3-4), 2006, 328-46.

4. Sajevic T, Leonardi A, Krizaj I. Haemostatically active proteins in snake venoms, *Toxicon*, 57(5), 2011, 627-45.

5. Gasanov S E, Dagda R K, Rael E D. Snake Venom Cytotoxins, Phospholipase As, and Zn-dependent Metalloproteinases: Mechanisms of Action and Pharmacological Relevance, *J ClinToxicol,* 4(1), 2014, 1000181.

6. Huang K F, Chiou S H, Ko T P, Wang A H. Determinants of the inhibition of a Taiwan habu venom metalloproteinase by its endogenous inhibitors revealed by X-ray crystallography and synthetic inhibitor analogues, *Eur J Biochem,* 269(12), 2002, 3047-56.

7. Mendes M M, Vieira S A, Gomes M S, Paula V F, Alcantara T M, Homsi-Brandeburgo M I,dos Santos J I, Magro A J, Fontes M R, Rodrigues V M. Triacontyl p-coumarate: an inhibitor of snake venom metalloproteinases, *Phytochemistry,* 86, 2013, 72-82.

8. Gutierrez J M, Rucavado A, Escalante T, Diaz C. Hemorrhage induced by snake venom metalloproteinases: biochemical and biophysical mechanisms involved in microvessel damage, *Toxicon,* 45(8), 2005, 997-1011.

9. Markland F S. Snake venoms and the hemostatic system, *Toxicon,* 36(12), 1998, 1749-800.

10. Kini R M, Evans H J. Structural domains in venom proteins: evidence that metalloproteinases and nonenzymatic platelet aggregation inhibitors (disintegrins) from snake venoms are derived by proteolysis from a common precursor, *Toxicon,* 30(3), 1992, 265-93.

11. Escalante T. Ortiz N, Rucavado A, Sanchez E F, Richardson M, Fox J W, Gutiérrez J M. Role of collagens and perlecan in microvascular stability: exploring the mechanism of capillary vessel damage by snake venoms, *metalloproteinases PLoS One,* 6(12), 2011, e28017.

12. Bjarnason J B, Fox J W. Hemorrhagic metalloproteinases from snake venoms, *Pharmacol Ther,* 62(3), 1994, 325-72.

13. Rucavado A. Nunez J, Gutierrez J M. Blister formation and skin damage induced by BaP1, a haemorrhagic metalloproteinase from the venom of the snake Bothropsasper, *Int J ExpPathol, 79*(4), 1998, 245-54.

14. José María Gutiérrez, Teresa Escalante, Alexandra Rucavado, Cristina Herrera. Hemorrhage Caused by Snake Venom Metalloproteinases: A Journey of Discovery and Understanding, *Toxins,* 8(4), 2016, 93

15. Kamiguti A S, Rugman F P, Theakston R D, Franca F O, Ishii H, Hay C R. The role of venom haemorrhagin in spontaneous bleeding in Bothropsjararaca envenoming. Butantan Institute Antivenom Study Group, *ThrombHaemost,* 67(4), 1992, 484-8.

16. Escalante T, Nunez J. Moura da Silva A M, Rucavado A, Theakston R D, Gutierrez J M. Pulmonary hemorrhage induced by jararhagin, a metalloproteinase from Bothropsjararaca snake venom, *ToxicolApplPharmacol,* 193(1), 2003, 17-28.

17. Han S M, Weaver F A, Comerota A J, Perler B A, Joing M. Efficacy and safety of alfimeprase in patients with acute peripheral arterial occlusion (PAO), *J VascSurg,* 51(3), 2010, 600-9.

18. Takeda S, Takeya H, Iwanaga S. Snake venom metalloproteinases: structure, function and relevance to the mammalian ADAM/ADAMTS family proteins, *BiochimBiophysActa,* 1824(1), 1824, 164-76.

19. Baramova E N, Shannon J D, Bjarnason J B, Fox J W. Degradation of extracellular matrix proteins by hemorrhagic metalloproteinases, *Arch BiochemBiophys,* 275(1), 1989, 63-71.

20. Kim Baeten and Katerina Akassoglou. Extracellular Matrix and Matrix Receptors in Blood Brain Barrier Formation and Stroke, 71(11), 2011, 1018-39.

21. Chinnasamy S, Chinnasamy S, Nagamani S, Muthusamy K. Identification of potent inhibitors against snake venom metalloproteinase (SVMP) using molecular

docking and molecular dynamics studies, *J BiomolStructDyn,* 33(7), 2014, 1516-27.

22. Muthusamy K, Chinnasamy S, Nagarajan S, Sivaraman T, Chinnasamy S. Isolation and characterization of bioactive compounds of *Clematis gouriana*Roxb. ex DC against snake venom phospholipase A(2) (PLA(2)) computational and in vitro insights, *J BiomolStructDyn,* 28, 2016, 1-14.

23. Cho A E, Guallar V, Berne B J, Friesner R. Importance of accurate charges in molecular docking: quantum mechanical/molecular mechanical (QM/MM) approach, *J ComputChem,* 26(9), 2005, 915-31.

24. Singh K D, Muthusamy K. Molecular modeling, quantum polarized ligand docking and structure-based 3D-QSAR analysis of the imidazole series as dual AT(1) and ET(A) receptor antagonists, *ActaPharmacol Sin,* 34(12), 2013, 1592-606.

25. Kirubakaran P, Arunkumar P, Premkumar K, Muthusamy K. Sighting of tankyrase inhibitors by structure- and ligand-based screening and *in vitro* approach, *MolBiosyst,* 10(10), 2014, 2699-712.

26. Murphy R B, Philipp D M, Friesner R A. A mixed quantum mechanics/molecular mechanics (QM/MM) method for large-scale modeling of chemistry in protein environments, *J ComputChem,* 21(16), 2000, 1442-57.

27. Tripathi S K, Singh S K. Insights into the structural basis of 3, 5-diaminoindazoles as CDK2 inhibitors: prediction of binding modes and potency by QM-MM interaction, MESP and MD simulation, *MolBiosyst,* 10(8), 2014, 2189-201.

28. Jorgensen W L, Maxwell D S, Tirado-Rives J. Development and testing of the OPLS all-atom force field on conformational energetics and properties of organic liquids, *J. Am. Chem. Soc,*118(45), 1996, 11225-11236.

29. Bowers K J, Shaw Res. LLC, New York, NY. Chow, E. Huageng, X u. Dror. Scalable Algorithms for Molecular Dynamics Simulations on Commodity Clusters, *Tampa, Florida,* 2006. 0-7695-2700-0/06.

30. Kaminski G A, Friesner R A, Tirado-Rives J, Jorgensen W L. Evaluation and reparametrization of the OPLS-AA force field for proteins via comparison with accurate quantum chemical calculations on peptides, *J PhysChem B,* 105(28), 2001, 6474-6487.

31. Cao H, Pan X, Li C, Zhou C, Deng F, Li T. Density functional theory calculations for resveratrol, *Bioorg Med ChemLett,* 13(11), 2003, 1869-71.